

Temporal Variation of the Coronal Parameter in a Jetted Tidal Disruption Event: Swift J1644+57

ARKA CHATTERJEE,^{1,2} KIMITAKE HAYASAKI,^{3,4} PRANTIK NANDI,^{5,6} NEERAJ KUMARI,⁷ SKYE R. HEILAND,⁸
ARGHAJIT JANA,⁹ SACHINDRA NAIK,⁵ AND SAMAR SAFI-HARB²

¹*Department of Physics, School of Advanced Engineering, UPES, Dehradun, 248007, India*

²*Department of Physics & Astronomy, Faculty of Science, University of Manitoba, Winnipeg, Manitoba, R3T 2N2, Canada*

³*Department of Astronomy and Space Science, Chungbuk National University, Cheongju, 361-763, Republic of Korea*

⁴*Department of Physical Sciences, Aoyama Gakuin University, Sagamihara 252-5258, Japan*

⁵*Physical Research Laboratory, Navrangpura, Ahmedabad, 380009, India*

⁶*Indian Centre for Space Physics, Barakhola, Netaji Nagar, Kolkata, 700099 India*

⁷*Indian Institute of Astrophysics, Koramangala, Bengaluru 560 034, India*

⁸*Department of Physics & Astronomy, University of British Columbia, Vancouver, BC, V6T 1Z4, Canada*

⁹*Department of Physics, SRM University-AP, Amaravati, Andhra Pradesh 522240, India*

ABSTRACT

Tidal Disruption Events are exotic astrophysical phenomena where matter from a star or the interstellar medium is captured by a supermassive black hole. The process liberates enormous energy, within a few months to a year timescale, enough to detect dormant black holes in near as well as the farthest galaxies. We revisit the long-term spectral variabilities associated with the jetted Tidal Disruption Event *Swift* J1644+57 by exploring the archival X-ray data obtained with MAXI/GSC, Swift/XRT, and XMM-Newton observatories. Our analysis reveals that the spectral indices decrease non-monotonically as *Swift* J1644+57 evolves with time. We also find that the soft (0.3-1.5 keV) and hard (1.5-10 keV) X-ray photon counts are highly correlated with a maximum correlation coefficient of 0.95 and peak at *zero* lag. Moreover, the soft and hard band variabilities obtained from XMM-Newton observations are highly correlated with a Pearson cross-correlation coefficient of 0.96. This indicates that the soft and hard X-ray photons are emitted from the same site, which is most likely a Compton cloud, i.e., the corona. Assuming the hard X-ray photons originate from the corona, we find that the coronal parameter undergoes rapid expansion during the early phases when accompanied by a relativistic jet launching and subsequently evolves toward a state of saturation with minor fluctuations in the latter stages. The temporal variation of the coronal size is consistent with a simple theoretical conjecture. We also discuss the application of our analytical outcomes to other jetted and non-jetted tidal disruption events.

Keywords: Accretion — Black Hole Physics — Tidal Disruption Events — Radiative processes—
Individual: Swift J1644+57

1. INTRODUCTION

Most galaxies are thought to harbor supermassive black holes (SMBHs) within the mass range of $10^6 M_{\odot} \lesssim M_{\text{bh}} \lesssim 10^{10} M_{\odot}$ (Kormendy & Richstone 1995; Kormendy & Ho 2013). The mass of the SMBH has been estimated using the reverberation mapping

technique (Peterson et al. 2004), measuring the proper motion of stars orbiting around the SMBH, and the $M - \sigma_*$ relation, where the velocity dispersion of stars (σ_*) around the galactic bulge is correlated with the mass of the SMBH (M).

Tidal disruption events (TDEs) can provide a unique way to probe the dormant SMBHs in inactive galaxies. A star is tidally disrupted when it reaches within the tidal disruption radius $R_t = (M_{\text{bh}}/m_*)r_*$, where M_{bh} is the mass of the SMBH, m_* is the stellar mass, and r_* is the stellar radius.

The tidal disruption radius is expressed by

$$\frac{R_t}{r_g} \approx 50 \left(\frac{M_{\text{bh}}}{10^6 M_\odot} \right)^{-2/3} \left(\frac{m_*}{M_\odot} \right)^{-1/3} \left(\frac{r_*}{R_\odot} \right) \quad (1)$$

in units of the gravitational radius, $r_g = GM_{\text{bh}}/c^2$, where G is the gravitational constant, M_{bh} is the mass of the black hole, and c is the speed of light.

After tidal disruption of the star, the stellar debris falls toward the SMBH and releases its gravitational energy as radiation, generating a luminosity large enough to be comparable to the Eddington limit. According to the standard TDE theory (Rees 1988; see also Rossi et al. 2021 for a review), the resultant luminosity decays with time, following the power law of time $t^{-5/3}$, for a span of a few 100 days over the wide range of optical/UV to X-ray wavebands. It is a key observational feature that the light curve decays with $t^{-5/3}$. Though a significant number of TDEs can deviate from the standard $t^{-5/3}$ decay rate due to stellar internal structure (Lodato & Rossi 2011), orbital eccentricity (Hayasaki et al. 2013, 2016, 2018; Park & Hayasaki 2020; Zhong et al. 2023), and/or the penetration factor which is the ratio of the tidal disruption to pericenter radii (Guillochon & Ramirez-Ruiz 2013).

The first observational evidence of TDEs dates back to the 1990s (Bade et al. 1996) by the All-Sky Survey of the *ROSAT* satellite. Since then, through multi-wavelength campaigns, ~ 100 (Gezari 2021) have been discovered in a wide range of wavebands from radio to optical/UV to X-ray bands. While most TDEs have been observed in optical/UV wavelengths, ~ 10 TDEs have been detected simultaneously in the UV/optical and soft X-ray wavelengths. In addition to these thermal TDEs without a relativistic jet (so-called non-jetted TDEs), there have been so far four remarkable TDEs that accompany a relativistic jet (jetted TDEs), such as *Swift* J164449.3+573451 (hereafter, *Swift* J1644+57) (Levan et al. 2011; Bloom et al. 2011a,b; Burrows et al. 2011), *Swift* J2058+05 (Cenko et al. 2012), *Swift* J1112-8238 (Brown et al. 2015), and AT2022cmc (Andreoni et al. 2022).

The event rate of non-jetted TDEs is estimated to be $1 \times 10^{-5} \text{ yr}^{-1}$ per galaxy for a typical galaxy (Donley et al. 2002; Magorrian & Tremaine 1999; Wang & Merritt 2004), whereas the event rate of jetted TDEs is estimated $0.03 \text{ Gpc}^{-3} \text{ yr}^{-1}$ (Sun et al. 2015; De Colle & Lu 2020; Andreoni et al. 2022). Recent observations indicate that many *Changing look* active galactic nuclei (AGNs) have been associated with TDEs (Eracleous et al. 1995; Merloni et al. 2015; Ricci et al. 2020, 2021; Jana et al. 2021). This could

also potentially increase the population of TDEs with e-ROSITA (Merloni et al. 2012) in the future. These event rates indicate the remarkable scarcity of the jetted TDE population. However, the population of jetted TDEs estimated above indicates a relatively small beaming angle ($\leq 1^\circ$). Of late, the discovery of off-axis jetted TDEs, such as IGR J12580+0134 in the nucleus of NGC 4845 galaxy (Walter et al. 2011) and the subsequent radio emission (Lei et al. 2016) suggest that the TDEs, which emit hard X-rays with weak radio emission, can show a global property of X-ray TDEs. Several non-jetted, radio-emitting TDEs have also been detected (Alexander et al. 2020; Cendes et al. 2021). Moreover, the recently discovered association of astrophysical IceCube neutrinos with three TDE candidates (Stein et al. 2021; Hayasaki 2021) invoked a new era of multi-messenger astronomy of TDEs.

There are differences in X-ray spectral hardness between jetted TDEs and non-jetted TDEs. Non-jetted TDEs often exhibit softer spectra, where photon index $\Gamma > 2.5$ is associated with a thermal component (Komossa 2017). Contrary to that, jetted TDEs have much harder spectra with $\Gamma \leq 2$. In addition, no clear evidence of a thermal component could be observed from the X-ray spectral energy distribution (Mangano et al. 2016; Seifina et al. 2017). The domain of jetted TDEs began in March 2011 with the discovery of *Swift* J1644+57. The origin of high-energy γ -rays is traced back to a galaxy at $z = 0.35$ (Levan et al. 2011). The peak X-ray luminosity exceeded the Eddington limit with the inferred black hole mass $3 \times 10^6 M_\odot$ (Bloom et al. 2011b; Burrows et al. 2011; Levan et al. 2011). The source was detected in radio (Cendes et al. 2014; Berger et al. 2012; Zauderer et al. 2013), infra-red (Wiersema et al. 2012); X-rays (Reis et al. 2012; Saxton et al. 2012; González-Rodríguez et al. 2014; Mangano et al. 2016; Zauderer et al. 2013), γ -rays (Bloom et al. 2011b; Burrows et al. 2011). Unlike X-ray luminosity, which decayed over the next 500 days, the radio luminosity increased (Berger et al. 2012; Zauderer et al. 2013)).

A quasi-periodic oscillation (QPO) of around 200 s within the first 20 days from the peak was discovered from the X-ray light curves in the 2-10 keV energy band from *Suzaku* and *XMM-Newton* observations (Reis et al. 2012; Saxton et al. 2012). Similar QPOs in X-rays have been observed for two other TDE candidates, namely 2XMM J123103.2+110648 (Lin et al. 2013) and ASASSN-14li (Pasham et al. 2019). Seifina et al. (2017) showed that the spectral hardness of the source evolved from $\Gamma \sim 1.8$ to $\Gamma \sim 1.2$ for the first 200 days since the outburst. However, the variation of spectral index

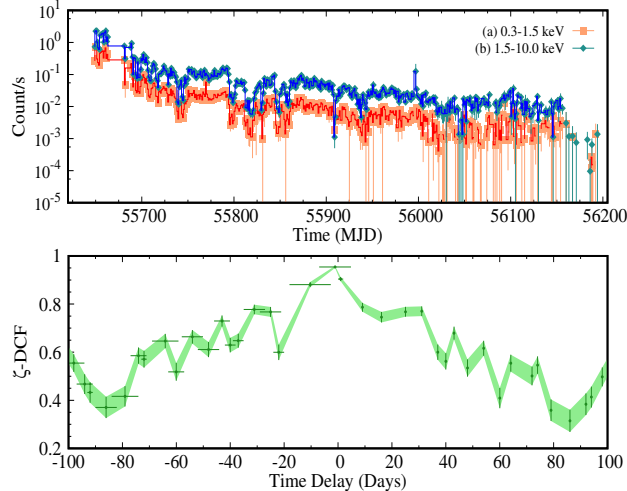


Figure 1. *Upper Panel:* X-ray light curves of Swift J1644+57, obtained from the *Swift*/XRT, are presented for 0.3–1.5 keV (square-light-salmon) and 1.5–10 keV energy bands (diamond-greenish-blue points). *Lower panel:* ζ -DCF cross-correlation between 0.3-1.5 keV and 1.5–10 keV ranges are presented for Swift J1644+57 using *Swift*/XRT data. Both the energy bands are highly correlated ($\rho_{max} = 0.95$). Considering the error bars, no delay is observed between the two X-ray bands.

met sudden variations associated with the dips found in the light curve (Mangano et al. 2016). From the X-ray spectral shape, luminosity, and the absence of the thermal component, Zauderer et al. (2013) asserted that the X-ray photons of *Swift* J1644+57 could not have originated from the accretion disk. Rather, the origin of the X-rays could be from the internal dissipation within the jet at a large distance ($r \sim 10^4 - 10^5 r_g$) from the SMBH. Contrary to their idea, Lei et al. (2016) suggested the X-rays from the off-axis jetted-TDE candidate IGR J12580+0134 is the disk-corona origin. Stronger evidence of the X-ray origin of *Swift* J1644+57 came from Kara et al. (2016), where reverberation lag was observed. Similar to the QPO detection of *Swift* J1644+57, Nikolaĵuk & Walter (2013) suggested detection of QPO within 0.0008-0.004 Hz, which is consistent with a black hole of mass $\sim 10^5 M_\odot$.

There are many arguments that the QPOs can bridge the mass gap between the accretion processes of galactic, stellar-mass black holes, and SMBHs (Vaughan & Uttley 2005). However, very few of them are detected with statistical confidence for AGNs (Gierliński et al. 2008; Alston et al. 2015; Ashton & Middleton 2021). There are many challenges for observing QPOs originating from AGNs, apart from achieving a statistically significant *signal to noise ratio* (Vaughan & Uttley 2006). Considering the mass of *Swift* J1644+57, the 200 s QPO found in the X-ray light curve requires a scale of $\mathcal{O}(10) r_s$ for a non-rotating SMBH. This scale fits within the range of the typical coronal size of TDEs as proposed by Mummery & Balbus (2021), and is also consistent with the corona size, which is observationally suggested for

many AGNs (Alston et al. 2020). Thus, we expect to find a reasonable explanation of hard X-ray variations through the disk-corona geometry by analyzing the existing data of jetted TDEs. The most promising mechanism for the luminous emission of TDEs is a thermal blackbody emission. Gezari (2021) suggested that there is a bimodal distribution of the TDE thermal emission, indicating that the soft X-ray photons are produced from the inner disk region, whereas the optical/UV photons are emitted from the outflow’s photosphere. The thermal photons produced from the disk can be a good candidate source for the Compton scattering. This suggests a disk-corona system can exist in X-ray TDEs.

Galeev et al. (1979) first proposed the disk-corona system to explain the hard X-ray origin of Galactic X-ray binaries. They formulated it based on an analogy with the solar coronal structure. The corona is heated through the magnetic reconnection at the disk surface and also through the convection within an accretion disk. As the inward flow progresses onto the black hole, the coronal structure can be dynamic, and the magnetic field strength increases, giving rise to a central cloud composed of hot electrons ($\sim 10^8$ K) and a magnetic field strength of the order of 10^7 Gauss. This model can explain the hard X-ray emission from Cyg X-1. Haardt & Maraschi (1991) proposed a two-phase component model, where the standard accretion disk surrounding the corona emits the soft photons, which are also reprocessed in the corona via Comptonization and reflection. The model was able to explain the general features of AGNs spectra. Subsequently, Martocchia & Matt (1996) and Miniutti & Fabian (2004) proposed the *Lamppost*

model, which includes the effect of the gravitational bending due to the black hole spin and the reflection effect by the iron $K\alpha$ line (Fabian & George 1991; Tanaka et al. 1995). Moreover, Liu et al. (2002) constructed a simple theoretical disk-corona model, where the corona is heated by magnetic reconnection and cooled by Compton scattering. The origin of the very high-temperature corona was considered to be the magnetic field for all of the above-mentioned models. More recently, Done et al. (2012) provided a more observationally consistent model *Optxagnf*. This model provides a spectral fit originating from the corona and disk with sub to super-Eddington accretion flows of AGNs. Their model also provides a practical estimate for the coronal size. In the TDE context, Mummery & Balbus (2021) applied the simple empirical model, where the corona expands as the luminosity decays and the smallest coronal size corresponds to the peak luminosity, to model the hard X-ray profile seen in the six non-jetted TDEs.

In this paper, we study how the Compton cloud of the jetted TDE *Swift* J1644+57 varies with time by using the *Optxagnf* model and whether the model can explain the hard X-ray properties. The paper is structured in the following way. In Section 2, we explain the data analysis method and the subsequent processing. In Section 3, we describe our results obtained from data analysis. We then discuss our findings and the implications on TDEs in Section 4. Finally, we summarize our conclusions in Section 5.

2. DATA ANALYSIS PROCESS

We used the archival data of *XMM-Newton* and *Swift*/XRT obtained through HEASARC¹. We reprocessed all data using `HEASOFT v6.26.1` (Arnaud 1996), which includes `XSPEC v12.10.1f`. We use the following cosmological parameters in this work: $H_0 = 70$ km s⁻¹ Mpc⁻¹, $\Lambda_0 = 0.73$, $\Omega_M = 0.27$ (Bennett et al. 2003). With the cosmological parameters, the luminosity distance of *Swift* J1644+57 was considered 1408 Mpc (Levan et al. 2011).

2.1. *Swift*/XRT

The X-ray telescope (XRT) (Burrows et al. 2005) on board *Swift* has the highest cadence monitoring observation of *Swift* J1644+57 in the X-ray band (0.3 to 10.0 keV), especially during the TDE from 2011. Depending on the brightness of the source, XRT observed this source in both Window Timing (WT) and Photon Counting (PC) modes. The source was observed by

Swift/XRT over ~ 500 times from 2011-03-31 to 2012-09-30. We stacked all observations into 17 segments depending on the brightness of the source. When the event started, the source was brighter. Thus, we stacked ~ 15 observations into a single spectrum and produced the combined spectrum. This procedure is followed for the first 154 observations. We stacked these observations into 10 combined observations (XRT1 to XRT10) (details are given in Table 1). After that, the source became dimmed with respect to previous observations. For that, we stacked ~ 40 observations into a single spectrum. This process is followed for the next 250 observations and produces the stacked spectrum from XRT11 to XRT15 (see Table 1). After 2012-03-17, we stacked 176 observations and 108 observations into a combined observation for XRT16 and XRT17, respectively. We use the online tool “XRT product builder”² (Evans et al. 2009) to extract the spectrum and light curves. This product builder performs all necessary processing and calibration and produces the final spectra and light curves of *Swift* J1644+57 WT and PC modes. The GRPPHA task is used with 10 counts per bin for XRT spectra. For more details, see Table 1.

2.2. *XMM-Newton*

We reprocessed the *XMM-Newton* Epic-pn data using the Science Analysis Software (SAS) v17.0.0 and updated calibration files. We reprocessed the data with the “eproc” task. For each observation ID, we created good time interval (GTI) files after eliminating the intervals of flaring particle background based on the count rate in the light curves above 10 keV. We filtered the event lists to get the good events with a pattern ≤ 4 for a given GTI file and generated the cleaned event lists. We extracted source and background spectra using circular regions of radii 30 and 50 arcsec, respectively. We generated the light curves in 0.2 – 2 keV and 3 – 10 keV ranges with 10 s time bin and corrected from effects like vignetting, bad pixels, and variations in PSF. We also checked for any pile-up effects in the data. We generated the redistribution matrix and ancillary response files using the SAS tasks “rmfgen” and “afrgen”, respectively. We grouped the spectrum with a minimum of 20 counts per bin and oversampled it by a factor of 3 using the “specgroup” task.

3. RESULTS

3.1. *Light curves*

¹ <http://heasarc.gsfc.nasa.gov/>

² http://swift.ac.uk/user_objects/

Table 1. Observation log for *Swift*/XRT and *XMM-Newton* observations of *Swift* J1644+57.

ID	Date (yyyy-mm-dd)	Obs. ID	Instrument	Total Exposure (ks)
XRT1	2011-03-31	00031955002	<i>Swift</i> /XRT	224
	-2011-04-14	-00031955016		
XMM1	2011-03-31	0658400701	<i>XMM-Newton</i> /Epic-pn	26
XRT2	2011-04-15	00031955017	<i>Swift</i> /XRT	210
	-2011-04-30	-00031955032		
XMM2	2011-04-16	0678380101	<i>XMM-Newton</i> /Epic-pn	25
XMM3	2011-04-30	0678380201	<i>XMM-Newton</i> /Epic-pn	29
XRT3	2011-05-01	00031955033	<i>Swift</i> /XRT	137
	-2011-05-13	-00031955047		
XRT4	2011-05-14	00031955048	<i>Swift</i> /XRT	162
	-2011-05-29	-00031955063		
XMM4	2011-05-16	0678380301	<i>XMM-Newton</i> /Epic-pn	30
XRT5	2011-05-30	00031955064	<i>Swift</i> /XRT	125
	-2011-06-12	-00031955078		
XMM5	2011-05-30	0678380401	<i>XMM-Newton</i> /Epic-pn	30
XRT6	2011-06-13	00031955079	<i>Swift</i> /XRT	131
	-2011-06-26	-00031955093		
XRT7	2011-06-27	00031955094	<i>Swift</i> /XRT	142
	-2011-07-13	-00031955109		
XMM6	2011-07-03	0678380501	<i>XMM-Newton</i> /Epic-pn	19
XRT8	2011-07-14	00031955110	<i>Swift</i> /XRT	80
	-2011-07-28	-00031955124		
XMM7	2011-07-15	0678380601	<i>XMM-Newton</i> /Epic-pn	30
XMM8	2011-07-15	0678380701	<i>XMM-Newton</i> /Epic-pn	19
XRT9	2011-07-29	00031955125	<i>Swift</i> /XRT	77
	-2011-08-12	-00031955139		
XRT10	2011-08-13	00031955140	<i>Swift</i> /XRT	56
	-2011-08-27	-00031955154		
XMM9	2011-08-14	0678380801	<i>XMM-Newton</i> /Epic-pn	29
XMM10	2011-08-27	0678380901	<i>XMM-Newton</i> /Epic-pn	30
XRT11	2011-08-28	00031955155	<i>Swift</i> /XRT	108
	-2011-10-01	-00031955190		
XMM11	2011-09-06	0678381001	<i>XMM-Newton</i> /Epic-pn	28
XMM12	2011-09-06	0678381101	<i>XMM-Newton</i> /Epic-pn	28
XMM13	2011-10-02	0678381201	<i>XMM-Newton</i> /Epic-pn	28
XRT12	2011-10-03	00031955191	<i>Swift</i> /XRT	110
	-2011-11-11	-00031955230		
XRT13	2011-11-12	00031955231	<i>Swift</i> /XRT	132
	-2011-12-21	-00032200015		
XRT14	2011-12-22	00032200016	<i>Swift</i> /XRT	104
	-2012-01-30	-00032200055		
XRT15	2012-01-31	00032200056	<i>Swift</i> /XRT	116
	-2012-03-17	-00032200100		
XRT16	2012-03-18	00032200101	<i>Swift</i> /XRT	120
	-2012-06-07	-00032200175		
XRT17	2012-06-08	00032200101	<i>Swift</i> /XRT	156
	-2012-09-30	-00032526046		

The long-term X-ray light curve obtained from the *Swift* /XRT showed a high degree of variation during the TDE of *Swift* J1644+57. The source counts changed dramatically by orders of magnitude (see Fig. 1) within the span of ~ 600 days. We split the energy band of *Swift* into 0.3 – 1.5 keV & 1.5 – 10.0 keV ranges. As evident from Fig. 1 and Fig. 2, the hard band dominated the entire episode with sudden dips occasionally observed (Mangano et al. 2016).

We performed cross-correlation analysis using ζ -discrete cross-correlation function (ZDCF³, (Alexander 1997)) on the long-term light curve obtained from the *Swift* /XRT satellite. ζ -DCF method provides a better estimate of the cross correlation function (CCF) for unevenly sampled data sets and considers the non-linearity while interpolating the lightcures. The cross-correlation study yields an optimal correlation of the 0.3-1.5 keV and 1.5-10 keV energy bands, having a correlation coefficient $\rho_{max} = 0.95$. The correlation pattern peaked at a negative delay of 1.09 ± 5.9 days. Considering the measurement error, this could be considered as a zero-delay between the two energy bands of the X-ray. A similar zero-delay was also observed for an outbursting GBH, named XTE J1550-564, where a relatively smaller size of the accretion disk is attributed to the absence of any delay (Chatterjee et al. 2020). The light curve, along with the ζ -discrete cross-correlation are presented in Fig. 1.

From the light curve of *Swift* /XRT, we obtained the Hardness-Ratio (HR) as presented in Mangano et al. (2016) and Seifina et al. (2017). We found that the source counts in the hard band were always greater (see Fig. 2) than in the soft band. As the event progressed, the contribution of the hard band in the light curve also increased making harder spectra at the late time of the tidal disruption event. The left panel of Fig. 2 shows the ‘HR’-diagram obtained using the first 90 days of data.

Using *XMM-Newton* data, we calculated the fractional variability (F_{var}) (Edelson et al. 1996, 2001; Edelson & Malkan 2012; Nandra et al. 1997; Vaughan et al. 2003) in the 0.2–2 and 3–10 keV bands. The light curves (presented as x_i counts s^{-1}) contain uncertainties σ_i of length N with a mean μ and standard deviation σ , related by,

$$F_{var} = \sqrt{\frac{\sigma_{XS}^2}{\mu^2}}, \quad (2)$$

³ ZDCF: <http://www.weizmann.ac.il/particle/tal/research-activities/software>

where, σ_{XS}^2 is the excess variance (Nandra et al. 1997; Edelson et al. 2002). σ_{XS}^2 is defined as,

$$\sigma_{XS}^2 = \sigma^2 - \sigma_{err}^2, \quad (3)$$

where, σ_{err}^2 is the mean squared error. The σ_{err}^2 is given by,

$$\sigma_{err}^2 = \frac{1}{N} \sum_{i=1}^N \sigma_i^2. \quad (4)$$

The normalized excess variance is given by,

$$\sigma_{NXS}^2 = \frac{\sigma_{XS}^2}{\mu^2}. \quad (5)$$

The uncertainties in F_{var} and σ_{NXS} (Vaughan et al. 2003) are given by,

$$err(F_{var}) = \sqrt{\left(\sqrt{\frac{1}{2N} \frac{\sigma_{err}^2}{\mu^2 F_{var}}}\right)^2 + \left(\frac{1}{\mu} \sqrt{\frac{\sigma_{err}^2}{N}}\right)^2}, \quad (6)$$

and

$$err(\sigma_{NXS}^2) = \sqrt{\left(\sqrt{\frac{2}{N} \frac{\sigma_{err}^2}{\mu^2}}\right)^2 + \left(\sqrt{\frac{\sigma_{err}^2}{N} \frac{2F_{var}}{\mu}}\right)^2}. \quad (7)$$

Table 2 presents the results of our variability study in soft and hard bands. The excess variance or σ_{NXS}^2 yielded a negative value, which resulted in an imaginary fractional variability (F_{var}) for the XMM5 observation. The maximum of σ_{NXS}^2 or F_{var} is observed during XMM3. The F_{var} of the hard band is found to be higher than its softer counterpart for all XMM-Newton observations. We find the F_{var} between 0.2-2 keV and 3-10 keV, presented in the right panel of Fig. 2, are highly correlated with a correlation coefficient of 0.96.

3.2. Spectra

To understand the X-ray spectral properties of *Swift* J1644+57, we used the phenomenological model along with the physical model. During fitting, we employed stacked XRT spectra to obtain a broad idea of spectral variations. All errors are quoted with 90% confidence level, unless specified otherwise.

We started the spectral fitting with `powerlaw` model, and the model in XSPEC reads as: `TBabs*zTBabs*(powerlaw)`.

The galactic hydrogen column density (N_H) was kept frozen at $0.016 \times 10^{22} \text{cm}^{-2}$ throughout the entire spectral fitting process. The initial fits with the `powerlaw` model provide a good fit with $\chi_{red}^2 \sim 1$. Table 3.2.1

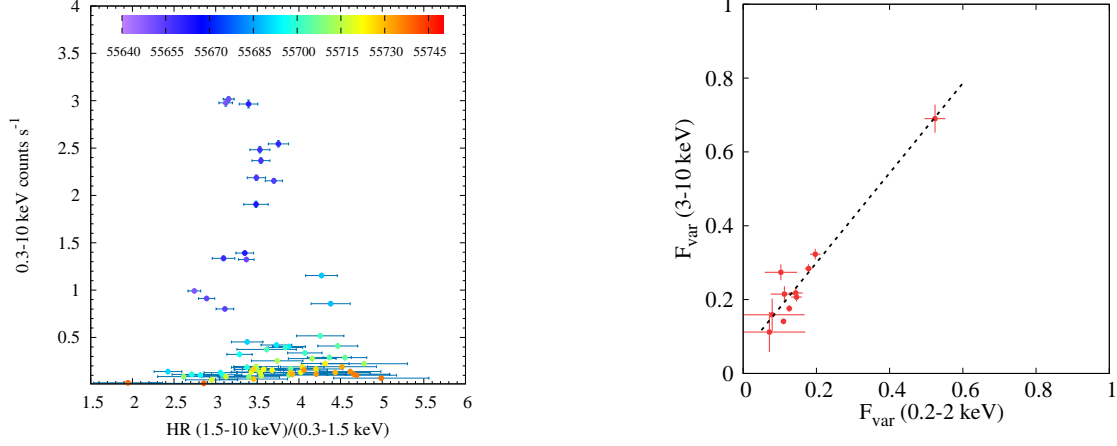


Figure 2. *Left Panel:* Hardness ratio of Swift J1644+57 is presented. The source exhibited hard spectra throughout the tidal disruption event. The colorbar on top represents the MJD from the start of the event. *Right Panel:* Correlated variability between 0.2–2 keV and 3–10 keV is observed from *XMM-Newton* data. The Pearson correlation coefficient is 0.96.

Table 2. Variability statistics in various energy ranges are shown in this table. We have opted for 100 sec time bins for variability analysis. In some cases, the average error of observational data exceeds the limit of 1σ , resulting in negative excess variance. In such cases, we have imaginary F_{var} , which are not shown in the table.

ID	Energy band keV	N	x_{max} Count/s	x_{min} Count/s	$\frac{x_{max}}{x_{min}}$	σ_{NXS}^2 (10^{-2})	F_{var} (%)
XMM1	0.2-2.0	451	8.34	3.69	2.26	1.21 ± 0.08	11.0 ± 0.51
XMM2	0.2-2.0	378	6.39	1.77	3.56	1.59 ± 0.16	12.6 ± 0.78
XMM3	0.2-2.0	301	1.46	0.02	60.8	27.4 ± 2.45	52.4 ± 2.83
XMM4	0.2-2.0	540	1.72	0.37	4.67	2.92 ± 3.19	17.8 ± 1.04
XMM5	0.2-2.0	302	0.30	0.03	11.8	-0.04 ± 2.95	--
XMM6	0.2-2.0	491	1.52	0.18	8.60	3.90 ± 0.50	19.7 ± 1.41
XMM7	0.2-2.0	322	1.01	0.13	8.00	2.06 ± 0.52	14.3 ± 1.92
XMM8	0.2-2.0	544	0.94	0.15	6.16	2.12 ± 0.41	15.6 ± 1.46
XMM9	0.2-2.0	513	0.36	0.03	14.3	0.51 ± 0.14	7.2 ± 9.80
XMM10	0.2-2.0	521	0.49	0.02	20.1	1.27 ± 0.84	11.2 ± 3.75
XMM11	0.2-2.0	386	0.43	0.02	17.3	0.63 ± 1.41	7.9 ± 8.89
XMM12	0.2-2.0	389	0.77	0.04	17.8	1.12 ± 0.91	10.3 ± 4.41
XMM1	3.0-10.0	451	6.57	2.25	2.93	2.01 ± 0.12	14.1 ± 0.63
XMM2	3.0-10.0	378	5.28	3.33	2.92	3.10 ± 0.22	17.6 ± 0.89
XMM3	3.0-10.0	300	1.62	0.02	66.6	44.7 ± 3.53	69.0 ± 3.80
XMM4	3.0-10.0	540	2.04	0.19	10.8	8.15 ± 0.47	28.4 ± 1.20
XMM5	3.0-10.0	299	0.26	0.03	10.1	-0.03 ± 0.03	--
XMM6	3.0-10.0	491	2.34	0.20	11.4	10.4 ± 0.63	32.3 ± 1.42
XMM7	3.0-10.0	322	1.36	0.26	5.31	4.81 ± 0.59	21.8 ± 1.60
XMM8	3.0-10.0	544	1.53	0.23	6.54	4.32 ± 0.41	20.7 ± 1.17
XMM9	3.0-10.0	513	0.36	0.03	14.0	1.30 ± 1.21	11.2 ± 5.41
XMM10	3.0-10.0	521	0.68	0.03	27.1	4.61 ± 0.86	21.5 ± 2.10
XMM11	3.0-10.0	389	0.44	0.03	17.3	2.54 ± 1.38	15.9 ± 4.40
XMM12	3.0-10.0	387	0.92	0.05	17.7	7.51 ± 1.05	27.4 ± 2.15

presents the findings of the fits. During the first observation, which spans from MJD 55651 to MJD 55665, the spectral index of the source was observed to be 1.79 ± 0.02 . Corresponding N_H was found to be $1.75 \pm 0.04 \times 10^{22} \text{cm}^{-2}$. The normalization of the `powerlaw` component was observed to be the highest $0.0177 \pm 0.005 \text{ ph cm}^{-2} \text{ s}^{-1}$ among all other observations. Our second observation was made by stacking *Swift* /XRT spectra within the duration of MJD 55666 to MJD 55681. The spectrum was fitted with a power law index $\Gamma = 1.62 \pm 0.01$ and corresponding N_H was found to be $1.44 \pm 0.03 \times 10^{22} \text{cm}^{-2}$. The normalization and flux, presented in Table 3.2.1, were found to be decreased compared to the first observation. This is consistent with the light curve. We found the highest reduced chi-square ($\chi_{red}^2 \sim 1.21$) for this particular observation. The fitted unfolded spectrum is presented in the left panel of Fig. 3. The following observation considered the stacked spectra within MJD 55682 to MJD 55694. The source flux decreased substantially in the XRT3 observation. We found a higher N_H compared to the previous observation. The spectral indices had increased in XRT4 and XRT5 compared to the previous observations, XRT2 and XRT3. Apart from that, the N_H had increased, and the corresponding flux decreased. We found a general trend of decreasing Γ up to XRT11. The corresponding N_H also increased, and the luminosity exhibited a decreasing pattern. The findings were comparable with the findings of Seifina et al. (2017). However, from XRT12, the spectral index started to increase. However, it should be noted that the errors corresponding to the spectral indices became larger as the source became dim and data quality was reduced. For XRT16 observation, we found the source spectrum showed a steeper Γ at 1.72 ± 0.22 , comparable to the initial days of the TDEs. The left Panel of Fig. 4 shows the 90% confidence contours of N_H and Γ . The spectral parameter variations, fitted with the `powerlaw` model, are presented in Fig. 5.

XMM-Newton observed *Swift* J1644+57 twelve times within the duration of the initial phase of the tidal disruption event ranging from MJD 55667 to MJD 55836. We fitted the *XMM-Newton* data with the `powerlaw` model to compare the parameter variations with the stacked observations created using *Swift* data. During the first observation, referred to as XMM1, we found that the source spectrum had a spectral index of 1.69 ± 0.01 with a relatively lower hydrogen column density of $1.29 \pm 0.01 \times 10^{22} \text{cm}^{-2}$. The `powerlaw` normalization and flux are found to be highest (see Table 3.2.1) in that particular observation. In the following observation, XMM2, the spectrum hardened

with $\Gamma = 1.54 \pm 0.01$ and associated N_H increased to $1.42 \pm 0.02 \times 10^{22} \text{cm}^{-2}$. The normalization and the flux were reduced substantially. Later, on MJD 55697, we fitted the XMM3 spectrum where Γ was found highest among all the *XMM-Newton* observations, having a value of 1.87 ± 0.05 . The flux decreased dramatically to -11.14×10^{-11} from $-10.15 \times 10^{-11} \text{ erg cm}^{-2} \text{ s}^{-1}$. This sudden dip in the flux could be associated with the dips found in the long-term light curve (Mangano et al. 2016; Seifina et al. 2017). During XMM4 observation, the source spectrum returned to a harder spectrum with $\Gamma = 1.55 \pm 0.02$. The concurrent flux increased from the previous observation. Later, in the XMM5 observation, we found an upward variation of the spectral index with $\Gamma = 1.59 \pm 0.08$. However, considering the error, the spectral index could be in a similar range as the XMM4 observation. The normalization and flux decreased rapidly, and the observed values are the lowest among all the *XMM-Newton* observations. Thereafter, both the flux and normalization increased with decreased spectral index. Post XMM5, the `powerlaw` fitted spectra exhibited a steady decrease in the flux with occasional variation in the spectral index. The source normalization also varied from 13.56×10^{-3} to $0.78 \times 10^{-3} \text{ ph cm}^{-2} \text{ s}^{-1}$ throughout the *XMM-Newton* observations.

The results obtained from the baseline `powerlaw` model, presented in Table 3.2.1, suggest a good fit using a single power law component. We found no residuals around the low energy part, which could indicate the presence of soft excess (Singh et al. 1985; Arnaud et al. 1985) or thermal component from the disk, often visible for X-ray TDE (Gezari 2021). The *Swift* and *XMM-Newton* data within the overlapping time broadly exhibited similar spectral variation with increasing N_H associated with decreasing spectral index. The overall flux of *Swift* J1644+57 decreased. We found a lower and more confined variation of N_H from the *XMM-Newton* observations as compared to the *Swift* observations. However, the variation of N_H from the observations with both satellites remained similar throughout the entire period. We did not find the presence of the iron $K\alpha$ line throughout the disruption event. The degrees of freedom for `powerlaw` fitting were higher for *Swift* observations compared to the *XMM-Newton* observations.

3.2.1. *Optxagnf*

The *Optxagnf* model, proposed by Done et al. (2012), provides an in-depth understanding of the spectral parameters as the parameters are generated from a physical picture of the accretion disk around the AGNs. The model-fitted parameters include the luminosity, coro-

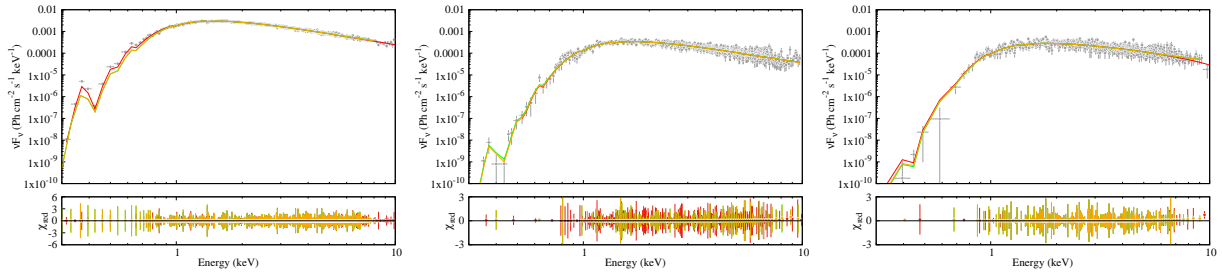


Figure 3. left to right: XRT2, XRT6, and XRT10 fitted unfolded spectra are presented for various models. The red line represents the `Optxagnf`, green represents the `Nthcomp`, and orange represents the `powerlaw` model. Corresponding residues are plotted in the bottom panels.

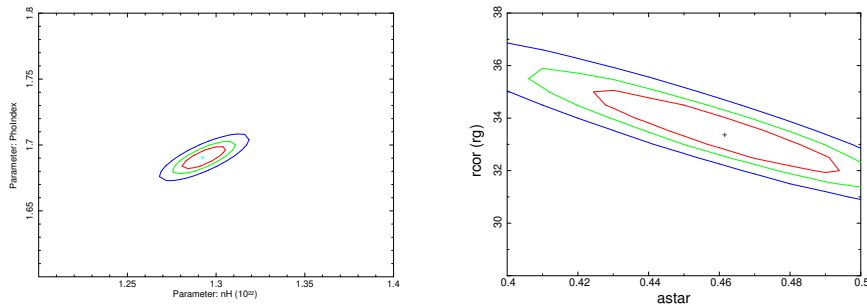


Figure 4. Contours of confidence are plotted for *Swift* /XRT observations fitted with `powerlaw` and `Optxagnf` model.

nal size, spin of the central black hole, soft-excess temperature, optical depth, spectral index, and the fraction of Comptonized photons. It should be noted that `Optxagnf` is the only publicly available model to fit the X-ray spectra of AGNs where coronal size could be estimated. We employed this model to fit the XRT spectra. The model in `xspec` reads as: `TBabs*zTBabs*(optxagnf)`.

The model spectrum computes both soft-excess and Comptonized photons. The accretion rate governed by the mass of the central black hole determines the luminosity of the spectra in units of Eddington luminosity. The geometry of the `Optxagnf` model separates the accretion disk into three regions. First, the disk emission is produced through a color temperature-corrected blackbody emission from radii $R_{\text{out}} > r > R_{\text{cor}}$, where R_{out} and R_{cor} are the outer edge of the disk and the corona, respectively. Second, at $r < R_{\text{cor}}$, the emission is dominated by Comptonized emission from a warm and optically thick medium. The third region where the inverse Comptonization occurs is in the optically thin corona located around the disk, and the fraction of inverse Comptonization could be estimated from the f_{pl} parameter while fitting the spectra. The temperature and optical depth of the warm, optically thick medium could be found from kT_s and τ , respectively. The model calculates the primary emission of Comptonized photons using the `Nthcomp` model, where the

seed photon temperature is kept fixed at $r = R_{\text{cor}}$, and the electron temperature of the optically thin hot corona is frozen at 100 keV. We freeze the mass of the black hole at $3 \times 10^6 M_{\odot}$ (Bloom et al. 2011b). The galactic N_H along the line of *Swift* J1644+57 remained frozen while performing the fitting. According to the model, it was suggested to keep the normalization frozen at unity. The redshift $z = 0.354$ and distance $d = 1402.8$ Mpc are also kept constant (Levan et al. 2011). From Tab 3.2.1, we can see that the power law model fits the spectra of *Swift* J1644+57 well, and the soft X-ray excess is absent in the spectra. Thus, we freeze the kT_s at 0.1 keV and τ at a maximum value of 5.0. Initially, we left the f_{pl} thawed. We observed that the f_{pl} values saturated for most of the cases. Later, better fits were obtained while fitting the spectra with variable kT_s and τ . We observed that the warm corona temperature and optical depth remained high for all of the observations except XRT3. We found that the kT_s gradually increases as the event progresses and remains within $0.59 \leq kT_s \leq 5.73$. On the other hand, the variation of optical depth remained non-monotonic within the limit $1.25 \leq \tau \leq 7.83$. The variation of f_{pl} remained within the range of $0.48 \leq f_{pl} \leq 0.93$ during our observation period. For TDEs, this is expected and is conjectured by Chakraborty et al. (2026). `Optxagnf` fitted spectra for three epochs are presented in Fig. 3, and the variation

of fitted parameters with time is plotted in the **right panel** of Fig. 5 and are presented in the Table 4.2.1.

We fitted the 0.3–10 keV stacked *Swift* spectra for the entire episode of TDE. The spectra fitted along with the `Optxagnf` model provided good statistics with $\chi_{red}^2 \sim 1$. The model-fitted spectral parameters are presented in Table 4.2.1. We found the luminosity of the source exceeded nearly 500 times the Eddington luminosity during the initial few days of the event. This agrees with the earlier studies like Zauderer et al. (2013) and is also seen from the current fitting with `Optxagnf` model. Over time, the luminosity of the source decreased nearly 200 times from the initial phase, but never went into the sub-Eddington regime during the period of our observation. The variation of N_H remained similar to what has been observed during the fitting with the `powerlaw` model. The spin of the central black hole remained within the range of $0.4 < a^* < 0.8$, making it an intermediate spinning black hole. During the initial days, the coronal parameter of the source was observed at $31 \pm 2 r_g$. The right panel of Fig. 4 represents the confidence contours of spin (a) vs coronal radius (r_{cor}). The coronal radius was found to vary within $31 < R_{cor} < 65 r_g$. We only used the stacked *Swift* data for `Optxagnf` fitting as it provides better data quality to understand long-timescale variations of *Swift* J1644+57 during its tidal disruption episode.

4. DISCUSSION

We studied *Swift* J1644+57 during its tidal disruption event of 2011-2012 using *Swift* and *XMM-Newton* data within the energy range 0.3-10 keV. We employed the `powerlaw` as our phenomenological model and a physical model, such as `Optxagnf`, to understand the behavior of the source as the event progresses. Being a jetted-TDE, the source exhibited variability in both the spectral and temporal domains and is one of the most studied tidal disruption events to date. During our analysis, we found that there are several similarities between TDEs and the declining phase of an outbursting GBH. The similarities between galactic black hole (GBH) transients and TDEs are seen from their spectral energy distributions and the decaying luminosity with time. The X-ray spectral indices of GBHs are found to decrease in the luminosity decay phase (McClintock et al. 2009). Likewise, the decreasing tendency of the spectral index has also been observed in *Swift* J1644+57 (Seifina et al. 2017). Recent *NICER* observations (Gendreau et al. 2012) of MAXI J1820+070 provided evidence of a dynamically contracting corona for the onset stage of the flare (Kara et al. 2019). Jana et al. (2016) explained, using the two-component

advective flow model (Chakrabarti & Titarchuk 1995), why the Compton cloud expanded at the declining phase of a low inclination GBH, MAXI J1836-194, during the 2011 outburst. The variation of the corona size is also observed for AGN IRAS 13224-3809 (Alston et al. 2020). Apart from coronal size variation, relativistic jet launching is another phenomenon that GBH transients and TDEs have in common (Mirabel & Rodríguez 1994; Patra et al. 2019; Espinasse et al. 2020; Blandford et al. 2019; Zauderer et al. 2011).

4.1. Nuclear Properties

X-ray emission from *Swift* J1644+57 has been observed for around 600 days. The hard X-ray component was found to dominate, and the radiation is conjectured to be beamed (Zauderer et al. 2013) and many authors. From our spectral analysis, we find that the source exhibited variations in hydrogen column density (N_H). Fig. 5, represents the variation of `powerlaw` fitted parameters. We find that the hydrogen column density, at the beginning, was higher at $1.75 \pm 0.04 \times 10^{22} \text{cm}^{-2}$. Later, in XRT2, the N_H dropped to $1.44 \pm 0.04 \times 10^{22} \text{cm}^{-2}$. Post XRT2, the spectra showed a gradual increase in the value of N_H and plateaued at a late stage. Similar observational findings are also seen through *XMM-Newton* spectra fitted with `powerlaw` model and *Swift* spectra fitted with the `Optxagnf` model. The variation of N_H could be a generic property of the jetted-TDEs.

Seifina et al. (2017) reported that the spectral index of individual spectra observed by *Swift* /XRT saturates after MJD 55730; i.e., after eighty days since the start of the event. We used stacked spectra of *Swift* /XRT where the spectral indices are observed to be decreasing up to MJD 55800. However, after that, the spectral indices increased. But, finally, at XRT17 observation, the spectral index was 1.28 ± 0.34 . Both *Swift* and *XMM-Newton* data are employed to measure the spectral indices variation within MJD 55650 to MJD 55800, where a similar pattern has been found. Using the `Optxagnf` model, we have also observed similar variations. The increase in the X-ray spectral indices after 150 days could be associated with the increased optical activity after $\sim 30 - 50$ days since the initial observations (Levan et al. 2016). We find that N_H and Γ are weakly anti-correlated with a Pearson Correlation coefficient of -0.22.

The `Optxagnf` model provides several parameters of the source. Among them, we find that the luminosity, in terms of $\log(L/L_{Ed})$, is highly sensitive to the fitting. The fitted spectra exhibited a variation of the order of 2 with the range of our observations. During the initial days, *Swift* J1644+57 had a bolometric luminosity

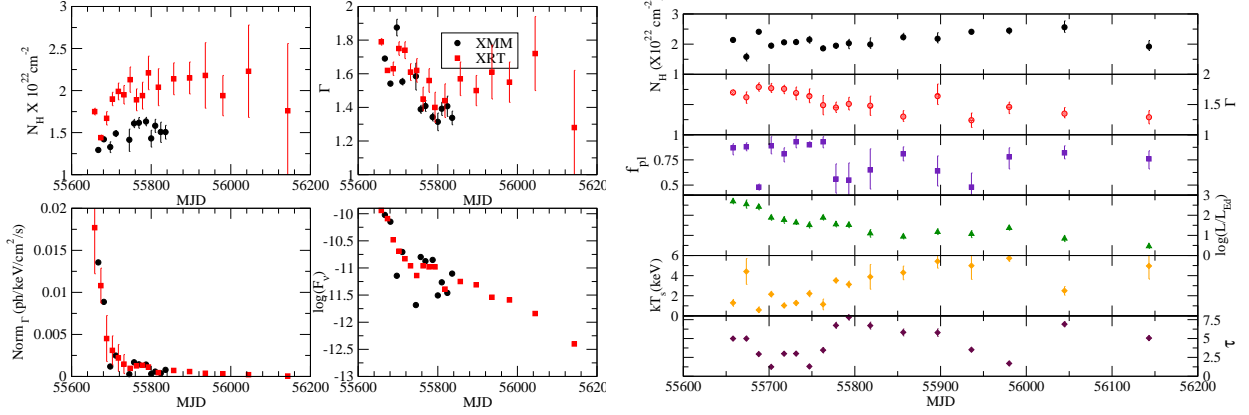


Figure 5. Variation of spectral parameters of Swift J1644+57 are presented for `powerlaw` and `optxagnf` model. Only stacked *Swift*/XRT data are employed to fit `optxagnf` model.

of around 500 times the Eddington limit. In the entire observation, the source luminosity was in the super-Eddington regime. The luminosity followed a steady decrease from the initial days, with occasional variation in between, which can be associated with the intrinsic photon count variation in the light curve. During XRT17, the last observation, the source luminosity decreased to nearly 3 times the Eddington limit. We find the source luminosity weakly correlated with the hydrogen column density, with a Pearson Correlation coefficient of -0.31.

The spin of *Swift* J1644+57, measured using the a^* parameter of `Optxagnf` model, exhibited a region of an intermediate spinning black hole. We find a^* to vary from 0.4 to 0.8. The value of the spin aligns with the earlier claim by Tchekhovskoy et al. (2014), where they predicted the spin of the source should be greater than ≥ 0.5 .

4.2. Coronal Variations

The hard X-ray photons, emerging from the vicinity of a black hole, are thought to originate from a corona which can be formed through magnetic reconnection in the accretion disk (Galeev et al. 1979; Liu et al. 2002). There are a few practical models of corona that have been proposed so far: *Lampost* model (Martocchia & Matt 1996; Miniutti & Fabian 2004) provides physical explanations of the X-ray spectra from the AGNs; Done et al. (2012) constructs `Optxagnf` model, computes the size of the corona, R_{cor} , from the spectral fitting. Also, it has been observed that the nature of the corona is dynamic for GBHs (Kara et al. 2019) and for the AGNs (Alston et al. 2020). That is why it is crucial to explore how the corona size evolves with time for TDEs.

To measure the coronal size variation of *Swift* J1644+57, we employ the `Optxagnf` model to determine the spectral fits using the stacked *Swift*/XRT data.

Through our spectral fitting, we find that at the peak luminosity of *Swift* J1644+57, the radial size of the corona was $31 \pm 2.3 r_g$. Subsequently, an almost similar size of the coronal parameter (R_{cor}) was found in the XRT2 and XRT3 observational epochs. The size of the corona increases $35 \pm 3.6 r_g$ in the XRT4 epoch. Later on, in the XRT5 and XRT6 epochs, the R_{cor} keeps increasing to $43 \pm 3.7 r_g$ and $51 \pm 4.3 r_g$, respectively. During the XRT7 observation, the R_{cor} is $58 \pm 4.1 r_g$. Up to the XRT7 observation, we observed a sharp rise in the R_{cor} . The fitted value of the R_{cor} is $61 \pm 4.2 r_g$ at XRT8 and drops to $58 \pm 4.5 r_g$ at XRT10. From the XRT10 to XRT17 observations, the R_{cor} varies little from $58 r_g$ to $64 r_g$, indicating a saturation level of the parameter. All estimated values of the coronal parameters are depicted in Fig. 8. In addition, we find through our analysis that the R_{cor} is anti-correlated with the luminosity $\log(L/L_{Edd})$ with the Pearson correlation coefficient: -0.87 .

Recently, Mummery & Balbus (2021) proposed the disk-corona model to explain non-thermal hard-X-ray emissions from X-ray TDEs. According to their prescription, the size of the corona would depend on the disk luminosity as follows:

$$R_{cor} = \begin{cases} R_I, & \text{initial size of corona,} \\ R_I + (R_C - R_I)f(l), & \text{intermediate size of corona,} \\ R_C, & \text{final size of corona,} \end{cases} \quad (8)$$

where

$$f(l) = \frac{l_I - l(t)}{l_I - l_C},$$

l_I , l_C , and $l(t)$ are the initial, final, and the time-dependent Eddington ratios, respectively. Starting with an initial coronal size R_I , the corona expands following the decay pattern of the luminosity profile and finally saturates to a value of R_C . We adopt $R_I = 30 r_g$

Table 3. powerlaw fitting result for the 0.3–10 keV energy range.

ID	MJD (days)	N_H (10^{22} cm^{-2})	Γ	N (10^{-3})	log(Flux) ($10^{-11} \text{ erg/cm}^2/\text{s}$)	χ^2/dof
<i>Swift</i> /XRT						
XRT1	55658	$1.75^{+0.04}_{-0.04}$	$1.79^{+0.02}_{-0.02}$	$17.7^{+5.50}_{-5.50}$	-09.94	902.74/827
XRT2	55673.5	$1.44^{+0.03}_{-0.03}$	$1.62^{+0.01}_{-0.01}$	$10.8^{+2.12}_{-2.12}$	-10.09	1047.47/861
XRT3	55688	$1.67^{+0.08}_{-0.08}$	$1.63^{+0.04}_{-0.04}$	$4.51^{+2.74}_{-2.74}$	-10.48	741.23/866
XRT4	55702.5	$1.90^{+0.08}_{-0.08}$	$1.75^{+0.04}_{-0.04}$	$3.10^{+1.73}_{-1.73}$	-10.63	525.19/703
XRT5	55717.5	$1.99^{+0.10}_{-0.10}$	$1.74^{+0.05}_{-0.05}$	$2.20^{+1.60}_{-1.60}$	-10.83	574.73/643
XRT6	55731.5	$1.95^{+0.11}_{-0.11}$	$1.61^{+0.05}_{-0.05}$	$1.47^{+1.13}_{-1.13}$	-10.96	615.79/640
XRT7	55747	$2.13^{+0.15}_{-0.15}$	$1.62^{+0.07}_{-0.07}$	$0.96^{+0.96}_{-0.96}$	-11.14	596.64/594
XRT8	55763	$1.89^{+0.13}_{-0.13}$	$1.45^{+0.07}_{-0.07}$	$1.26^{+0.12}_{-0.12}$	-10.96	555.14/596
XRT9	55778	$1.94^{+0.16}_{-0.16}$	$1.56^{+0.07}_{-0.07}$	$1.33^{+0.14}_{-0.14}$	-10.98	508.38/544
XRT10	55793	$2.21^{+0.20}_{-0.20}$	$1.40^{+0.09}_{-0.09}$	$1.12^{+0.15}_{-0.15}$	-10.98	498.03/520
XRT11	55818	$2.04^{+0.22}_{-0.22}$	$1.44^{+0.10}_{-0.10}$	$0.46^{+0.07}_{-0.07}$	-11.39	431.81/475
XRT12	55856.5	$2.14^{+0.19}_{-0.19}$	$1.57^{+0.10}_{-0.10}$	$0.72^{+0.09}_{-0.09}$	-11.25	466.99/509
XRT13	55896.5	$2.15^{+0.19}_{-0.19}$	$1.50^{+0.09}_{-0.09}$	$0.58^{+0.07}_{-0.07}$	-11.31	441.98/519
XRT14	55936	$2.18^{+0.39}_{-0.39}$	$1.61^{+0.16}_{-0.16}$	$0.38^{+0.10}_{-0.10}$	-11.54	274.05/309
XRT15	55980	$1.94^{+0.24}_{-0.24}$	$1.55^{+0.12}_{-0.12}$	$0.32^{+0.06}_{-0.06}$	-11.59	337.79/371
XRT16	56044.5	$2.23^{+0.55}_{-0.55}$	$1.72^{+0.22}_{-0.22}$	$0.21^{+0.08}_{-0.08}$	-11.84	166.80/197
XRT17	56143	$1.76^{+0.80}_{-0.80}$	$1.28^{+0.34}_{-0.34}$	$0.04^{+0.02}_{-0.02}$	-12.40	99.32/104
<i>XMM-Newton</i>						
XMM1	55667	$1.29^{+0.01}_{-0.01}$	$1.69^{+0.01}_{-0.01}$	$13.56^{+0.10}_{-0.10}$	-10.02	224.69/174
XMM2	55681	$1.42^{+0.02}_{-0.02}$	$1.54^{+0.01}_{-0.01}$	$8.87^{+0.10}_{-0.10}$	-10.15	186.68/173
XMM3	55697	$1.33^{+0.06}_{-0.06}$	$1.87^{+0.05}_{-0.05}$	$1.18^{+0.07}_{-0.08}$	-11.14	141.20/133
XMM4	55711	$1.49^{+0.04}_{-0.03}$	$1.55^{+0.02}_{-0.02}$	$2.48^{+0.07}_{-0.07}$	-10.71	193.00/167
XMM5	55745	$1.41^{+0.14}_{-0.13}$	$1.59^{+0.08}_{-0.08}$	$0.27^{+0.03}_{-0.03}$	-11.68	97.00/90
XMM6	55757	$1.61^{+0.05}_{-0.05}$	$1.39^{+0.02}_{-0.02}$	$1.68^{+0.06}_{-0.06}$	-10.80	186.57/162
XMM7	55769	$1.62^{+0.06}_{-0.06}$	$1.41^{+0.03}_{-0.03}$	$1.44^{+0.07}_{-0.06}$	-10.87	190.57/151
XMM8	55787	$1.63^{+0.05}_{-0.05}$	$1.34^{+0.02}_{-0.02}$	$1.41^{+0.05}_{-0.05}$	-10.85	179.59/163
XMM9	55800	$1.43^{+0.10}_{-0.10}$	$1.31^{+0.05}_{-0.05}$	$0.30^{+0.02}_{-0.02}$	-11.51	107.40/129
XMM10	55810	$1.58^{+0.08}_{-0.08}$	$1.39^{+0.04}_{-0.04}$	$0.58^{+0.03}_{-0.03}$	-11.26	154.57/145
XMM11	55824	$1.51^{+0.11}_{-0.12}$	$1.41^{+0.06}_{-0.06}$	$0.37^{+0.03}_{-0.03}$	-11.46	154.39/121
XMM12	55836	$1.51^{+0.08}_{-0.08}$	$1.34^{+0.04}_{-0.04}$	$0.78^{+0.04}_{-0.05}$	-11.10	167.89/144

and $R_C = 65 r_g$. The normalized disk luminosity, $\log(L/L_{\text{Edd}})$, at each observational epoch is displayed in Table 4.2.1. The predicted coronal size at each epoch using Equation (8) is denoted with red circles in Fig. 8. The error in the theoretical values is a contribution arising from the observational error in the measurement of luminosity as presented in Table 4.2.1. We find that the evolution of theoretically speculated corona size agrees with that of the observational R_{cor} parameter in *Swift* J1644+57, and considering the error bars, their variation remains similar.

Fig. 9 gives a schematic view of the disk-corona-jet system for the early and late stages of *Swift* J1644+57. The physical scale of the disk and corona fits within the range of $2R_t \sim 100 r_g$ for a $10^6 M_\odot$ SMBH, where R_t is given by Equation (1). We presume that, in the initial days, the accretion rate was at the super-Eddington rate, and the corona was small. As the days progressed, the accretion rate reduced, and the magnetic flux became stronger, as suggested by Tchekhovskoy et al. (2014). This allows the disk to have a bigger corona than that of the initial state. Although the disk is yet in the super-Eddington regime at this moment, the big-

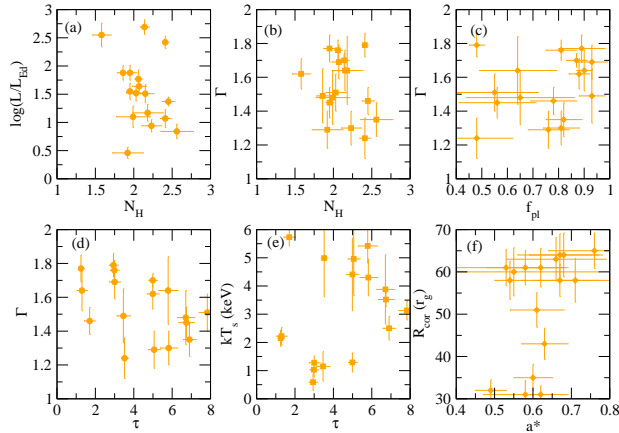


Figure 6. `Optxagnf` fitted spectral parameters variation with each other of Swift J1644+57 are presented. Panel (a) shows the variation of N_H with respect to the normalized luminosity. The variation of N_H with respect to Γ is shown in panel (b). Panel (c) demonstrates the weak correlation between Γ and scattering fraction f_{pl} . Variation of the Γ and τ can be observed in panel (d). Panel (e) presents the variation of coronal radius and spin parameter. Uncorrelated variation between spin and coronal radius can be observed in panel (e).

ger corona is likely to produce a larger number of high-energy X-ray photons via inverse Compton scattering. Within the first hundred days, the jet flux increases monotonically and is anti-correlated with the X-ray flux (Berger et al. 2012; Seifina et al. 2017), suggesting that the jet region also expands during this period. Depending on the quality and amount of the X-ray observational data, one can measure the coronal variation of the other three jetted TDEs and non-jetted TDEs using the same analysis as ours. This is also useful for improving the theoretical corona model in TDEs. More recently, Chakraborty et al. (2026) argued that the accretion disk of X-ray bright TDEs could be composed of a variable corona having lower electron temperature and higher optical depth, and can also be observed from the variation of parameters presented in Table 4.2.1.

4.2.1. Viability of TDE Corona Models

It should be noted that, to date, there exists no publicly available model in XSPEC to fit the hyper accretion regime of Swift J1644+57. The source was one of the very few jetted TDEs ever observed with a QPO feature. The initial accretion rate was $\sim 1000 L_{Edd}$ and was widely explored for its unique attributes. While choosing the model, one must be extremely cautious. `Optxagnf` is the only model in XSPEC that applies to the super-Eddington accretion regime of the AGNs, and measures the coronal size.

According to the `Optxagnf` model (Done et al. 2012), in the $r \leq r_{cor}$ region, the disk and the corona could co-exist to make a “disk-corona” structure (Galeev et al. 1979; Haardt & Maraschi 1991; Martocchia & Matt 1996; Liu et al. 2002), and such a configuration also provides higher photon interception to the corona. The

transition radius after which the radiation transfers from pure color-corrected black body to the inverse Comptonizations in the high τ & low kT_s and/or low τ & high kT_s regions is called the coronal radius. In reality, Compton up or down scattering in the radiation pressure supported torus is complex in nature (Kawaguchi 2003) due to the interplay between twisted magnetic field lines (Jiang et al. 2019) and the velocity field of electrons (Chatterjee et al. 2018). The Compton y-parameter is inadequate for interpreting Comptonized spectra in super-Eddington, jet-dominated accretion flows, as it assumes a thermal, homogeneous, isotropic electron plasma in the Thomson regime. In high- τ , advective, or non-thermal environments such as Swift J1644+57, y could become degenerate and physically misleading. Nevertheless, X-ray emission originated from the “disk-corona”, or corona was earlier suggested by Lei et al. (2016); Kara et al. (2016); Mangano et al. (2016). Moreover, the source exhibits Comptonized X-ray spectra with variable hardness that are well described by evolving Comptonization components, independent of the precise inner accretion flow geometry (Bloom et al. 2011a; Burrows et al. 2011).

Recently, Chakraborty et al. (2026) has proposed a coronal emission for TDEs (see their Fig. 7) where the optical depth could be higher, accompanied by a lower electron temperature. The parameters obtained from the `Optxagnf` model, presented in Table 4.2.1, exhibit a similar nature of corona. Although the morphology of the TDE corona could depart from the structure of the warm corona, the thermal properties, such as high τ and kT_s , resemble the warm corona of the `Optxagnf` model. The variation of coronal radius could be observed from the MCMC plots presented in the Fig. 7.

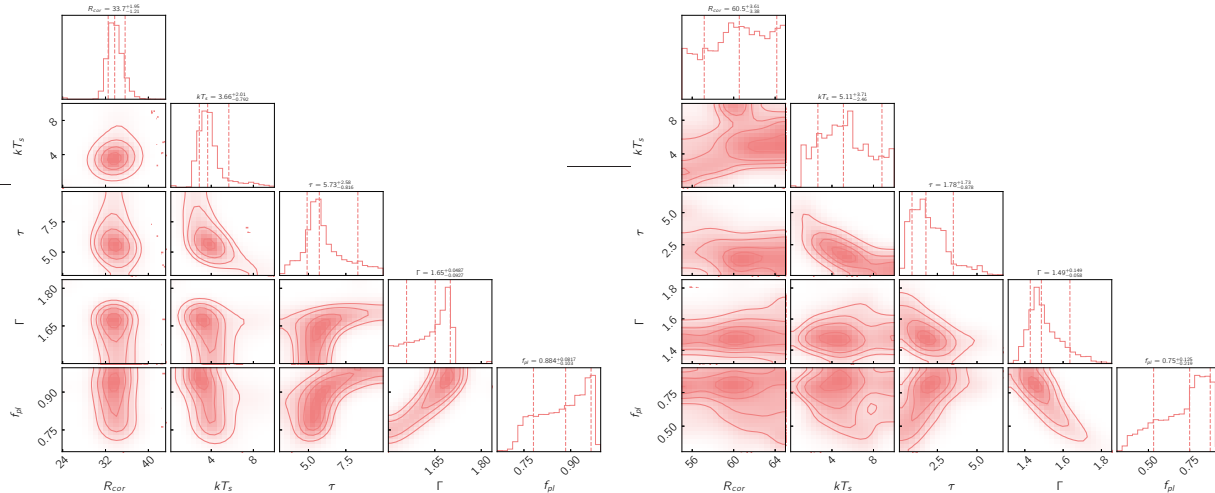


Figure 7. Markov Chain Monte-Carlo plot for parameter variations of XRT2 and XRT15 are presented. Goodman-Weare (EMCEE) (Foreman-Mackey et al. 2013) is opted for 32 walkers and a chain length of 1 million iterations, where the transient phase is removed by burning the chain up to 9984 iterations. The spin parameter was kept frozen at $a = 0.60$ to perform the MCMCs.

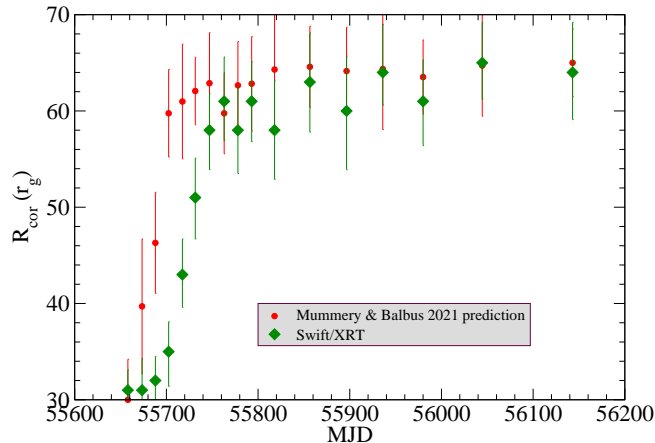


Figure 8. Coronal variation with time is presented for Swift J1644+57. *Swift* /XRT fitted values are presented by green-diamond points. The red circles denote the theoretical values of R_{cor} as predicted by Mummery & Balbus (2021).

However, it should be noted that `Optxagnf`, developed for AGNs, may not be physically self-consistent for hyper-Eddington jetted TDEs, such as for *Swift* J1644+57.

The high optical depth (τ) & low (kT_s) corona could form in the case of radiation pressure supported tori or super-Eddington thick disks, which were investigated by Abramowicz et al. (1978); Kozłowski et al. (1978); Abramowicz et al. (1980); Paczyński & Wiita (1980); Sikora (1981); Fukue (1982); Chakrabarti (1985a); Madau (1988); Ulmer (1997); Jiang et al. (2019); Jiang & Dai (2024). Thick disks are capable of launching collimated jets (Rees et al. 1982; Chakrabarti 1985b) and could also produce QPOs through oscillations (Jaroszynski 1986). The radiative properties of the TDEs need to be explored in this regime. However,

there are no models in XSPEC with the thick disk feature. Furthermore, under the ideal situation, one could be exploring the Magnetically Arrested Disks (MAD, Narayan et al. (2003); Tchekhovskoy et al. (2014)) to fit the broadband SED spectra of the jetted TDEs. In future work, we will incorporate a simplified thick disk model in XSPEC to examine the parameters for several X-ray bright TDEs.

5. SUMMARY

We have re-visited the X-ray emission of the jetted-TDE *Swift* J1644+57 between 2011 and 2012 by analyzing the archival *Swift* and *XMM-Newton* data with HEASoft. *Swift* J1644+57 showed a massive tidal disruption event during 2011 and 2012, where the flux of the hard (3–10 keV) photons dominated that of the soft

Table 4. `Optxagnf` fitted spectral parameter are presented. We used stacked *Swift*/XRT over *XMM-Newton* as the former provides more degrees of freedom over the latter.

ID	MJD (days)	N_H (10^{22}cm^{-2})	$\log(\frac{L_o}{L_E})$	a^*	r_{cor} (r_g)	kT_s (keV)	τ	Γ	f_{pt}	dof/χ^2
XRT1	55658	$2.14^{+0.06}_{-0.07}$	$2.69^{+0.13}_{-0.12}$	$0.62^{+0.03}_{-0.04}$	$31^{+2.1}_{-2.3}$	$1.29^{+0.34}_{-0.33}$	$4.99^{+0.23}_{-0.24}$	$1.70^{+0.04}_{-0.04}$	$0.87^{+0.04}_{-0.07}$	887/830
XRT2	55673.5	$1.58^{+0.12}_{-0.14}$	$2.55^{+0.21}_{-0.20}$	$0.58^{+0.11}_{-0.13}$	$31^{+3.3}_{-4.1}$	$4.41^{+1.29}_{-1.28}$	$4.99^{+0.31}_{-0.27}$	$1.62^{+0.09}_{-0.10}$	$0.88^{+0.04}_{-0.04}$	1058/938
XRT3	55688	$2.41^{+0.04}_{-0.03}$	$2.42^{+0.11}_{-0.15}$	$0.49^{+0.04}_{-0.06}$	$32^{+2.5}_{-2.2}$	$0.59^{+0.30}_{-0.25}$	$2.94^{+0.22}_{-0.22}$	$1.79^{+0.07}_{-0.07}$	$0.48^{+0.03}_{-0.03}$	722/689
XRT4	55702.5	$1.95^{+0.08}_{-0.07}$	$1.88^{+0.13}_{-0.13}$	$0.60^{+0.05}_{-0.04}$	$35^{+3.1}_{-3.6}$	$2.15^{+0.29}_{-0.26}$	$1.25^{+0.15}_{-0.15}$	$1.77^{+0.08}_{-0.07}$	$0.89^{+0.09}_{-0.08}$	625/703
XRT5	55717.5	$2.06^{+0.05}_{-0.05}$	$1.77^{+0.16}_{-0.17}$	$0.63^{+0.06}_{-0.06}$	$43^{+3.7}_{-3.4}$	$1.03^{+0.25}_{-0.22}$	$2.99^{+0.23}_{-0.25}$	$1.76^{+0.06}_{-0.08}$	$0.81^{+0.06}_{-0.08}$	575/646
XRT6	55731.5	$2.07^{+0.09}_{-0.08}$	$1.64^{+0.10}_{-0.10}$	$0.61^{+0.07}_{-0.06}$	$51^{+4.1}_{-4.3}$	$1.28^{+0.24}_{-0.26}$	$3.00^{+0.28}_{-0.28}$	$1.69^{+0.10}_{-0.11}$	$0.93^{+0.06}_{-0.06}$	683/638
XRT7	55747	$2.15^{+0.11}_{-0.12}$	$1.51^{+0.16}_{-0.15}$	$0.67^{+0.10}_{-0.10}$	$58^{+3.8}_{-4.1}$	$2.22^{+0.31}_{-0.32}$	$1.30^{+0.27}_{-0.27}$	$1.64^{+0.12}_{-0.11}$	$0.90^{+0.03}_{-0.02}$	593/587
XRT8	55763	$1.86^{+0.08}_{-0.06}$	$1.88^{+0.13}_{-0.12}$	$0.62^{+0.07}_{-0.08}$	$61^{+4.6}_{-4.1}$	$1.15^{+0.52}_{-0.54}$	$3.46^{+0.35}_{-0.36}$	$1.49^{+0.16}_{-0.16}$	$0.93^{+0.05}_{-0.06}$	550/594
XRT9	55778	$1.95^{+0.05}_{-0.09}$	$1.55^{+0.14}_{-0.13}$	$0.54^{+0.04}_{-0.04}$	$58^{+4.5}_{-4.5}$	$3.52^{+0.24}_{-0.24}$	$6.74^{+0.41}_{-0.38}$	$1.45^{+0.09}_{-0.08}$	$0.56^{+0.15}_{-0.14}$	510/547
XRT10	55793	$2.03^{+0.13}_{-0.18}$	$1.52^{+0.14}_{-0.14}$	$0.58^{+0.10}_{-0.10}$	$61^{+4.1}_{-4.2}$	$3.13^{+0.33}_{-0.33}$	$7.83^{+0.44}_{-0.39}$	$1.51^{+0.11}_{-0.10}$	$0.55^{+0.17}_{-0.17}$	511/527
XRT11	55818	$1.99^{+0.22}_{-0.13}$	$1.10^{+0.19}_{-0.19}$	$0.71^{+0.11}_{-0.15}$	$58^{+5.2}_{-5.1}$	$3.88^{+1.23}_{-1.23}$	$6.71^{+0.46}_{-0.46}$	$1.48^{+0.16}_{-0.16}$	$0.65^{+0.21}_{-0.19}$	426/463
XRT12	55856.5	$2.23^{+0.13}_{-0.09}$	$0.94^{+0.11}_{-0.12}$	$0.66^{+0.13}_{-0.09}$	$63^{+5.1}_{-5.2}$	$4.30^{+0.65}_{-0.71}$	$5.82^{+0.45}_{-0.47}$	$1.30^{+0.10}_{-0.08}$	$0.81^{+0.07}_{-0.07}$	444/461
XRT13	55896.5	$2.18^{+0.20}_{-0.14}$	$1.17^{+0.15}_{-0.13}$	$0.55^{+0.22}_{-0.16}$	$60^{+5.7}_{-6.1}$	$5.42^{+0.60}_{-0.68}$	$5.79^{+0.50}_{-0.51}$	$1.64^{+0.20}_{-0.14}$	$0.64^{+0.15}_{-0.15}$	440/508
XRT14	55936	$2.41^{+0.07}_{-0.07}$	$1.07^{+0.16}_{-0.18}$	$0.67^{+0.11}_{-0.12}$	$64^{+5.0}_{-3.4}$	$4.99^{+1.37}_{-1.37}$	$3.52^{+0.17}_{-0.17}$	$1.24^{+0.12}_{-0.12}$	$0.48^{+0.14}_{-0.13}$	246/300
XRT15	55980	$2.45^{+0.08}_{-0.11}$	$1.37^{+0.08}_{-0.11}$	$0.53^{+0.14}_{-0.10}$	$61^{+4.3}_{-4.6}$	$5.73^{+0.31}_{-0.33}$	$1.70^{+0.29}_{-0.31}$	$1.46^{+0.08}_{-0.11}$	$0.78^{+0.09}_{-0.09}$	329/368
XRT16	56044.5	$2.56^{+0.21}_{-0.17}$	$0.84^{+0.13}_{-0.15}$	$0.76^{+0.12}_{-0.10}$	$65^{+4.2}_{-3.8}$	$2.50^{+0.42}_{-0.44}$	$6.90^{+0.33}_{-0.33}$	$1.35^{+0.10}_{-0.07}$	$0.82^{+0.07}_{-0.06}$	166/192
XRT17	56143	$1.92^{+0.20}_{-0.13}$	$0.46^{+0.10}_{-0.10}$	$0.68^{+0.09}_{-0.08}$	$64^{+5.2}_{-4.9}$	$4.96^{+1.30}_{-1.30}$	$5.06^{+0.31}_{-0.32}$	$1.29^{+0.11}_{-0.11}$	$0.76^{+0.08}_{-0.10}$	99.5/100

(0.2–2 keV) photons over the entire period. We have hypothesized that those hard photons originate from the Compton cloud, i.e., the corona, and have estimated the size of the corona by measuring the size of the hard X-ray emitted region using the publicly available model `Optxagnf`. Our key findings are summarized as follows.

1. We find that the spectral index non-monotonically decreases with time, demonstrating that the fraction of harder photons increases with time. This

indicates that the size of the Compton cloud gets larger because the soft photons are more scattered to be exhausted. We observed that the optical depth (τ) and the temperature of the warm corona (kT_s) remained high – a result that aligns with the [Chakraborty et al. \(2026\)](#) study.

2. By interpreting the hard X-ray-emitted region as a corona, we have estimated the size of the corona as a function of time. We confirm that the coronal

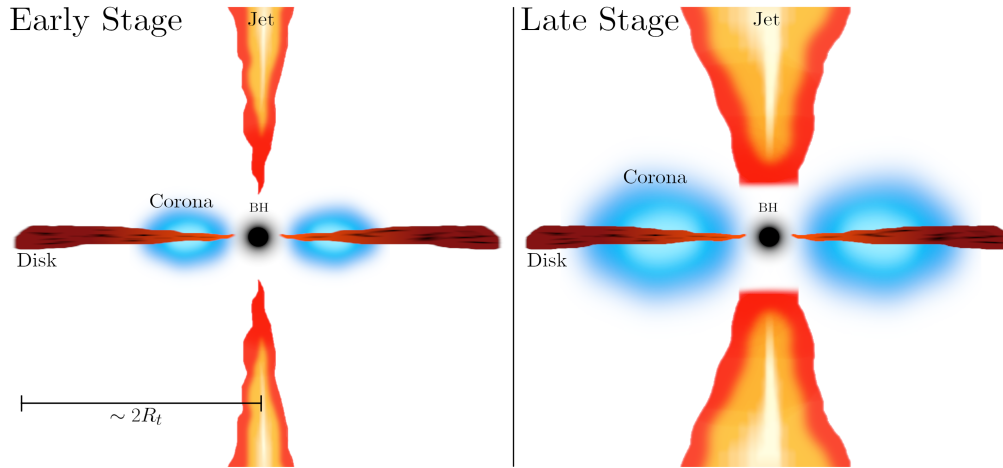


Figure 9. Edge-on view schematic diagram of coronal size variation in the early and late stages of *Swift* J1644+57. The system comprises a disk around the SMBH, a corona on the disk, and a jet. The disk size is twice the tidal disruption radii, which is approximately estimated to be $2R_t \sim 100 r_g$ for the $10^6 M_\odot$ SMBH and a solar-type star (see equation 1).

parameter increases over time for the observed period. We also find that the evolution of the corona size agrees with the theoretical conjecture made by Mummery & Balbus (2021).

3. We find that the flux of hard and soft photons is highly correlated with the correlation coefficient $\rho_{max} = 0.95$ throughout the event. Their correlation pattern has peaked at a zero delay. Moreover, the flux variabilities of the soft (0.2-2 keV) and hard (3-10 keV) photons correlate with each other with a Pearson correlation coefficient of 0.96. These correlations suggest that the soft and hard band photons are emitted from the same source.

Four jetted TDEs have been observed so far (Cenko et al. 2012; Brown et al. 2015; Andreoni et al. 2022). In the future, more exotic events could be observed by *XRISM* (Tashiro et al. 2018). The large field of view and imaging capability of the proposed-to-NASA mission *AXIS* (Mushotzky & AXIS Team 2019; Reynolds et al. 2023; Safi-Harb et al. 2023; Koss et al. 2025) could provide a detailed structure of the X-ray emitting region of these sources. Also, to perform the short-term timing studies and search for more QPOs among the AGNs, the large effective area and high throughput of the proposed-to-CSA *Colibrí* (Heyl et al. 2019; Caiazzo et al. 2019) and proposed-to-ESA *NewAthena* (Cruise et al. 2025) missions will be required in the future. Future proposed X-ray interferometric missions (Cash et al. 2000; Cash 2003; Gendreau et al. 2004; Chatterjee et al. 2017, 2018; Chatterjee 2018; Uttley et al., 2020; Gandhi 2023; Weaver et al. 2026) are essential to visualize the coronal

variation in the configuration space, much like what EHT (Event Horizon Telescope Collaboration et al. 2025) has obtained in the radio and sub-mm range.

- 1 The authors acknowledge an anonymous reviewer for
- 2 their constructive comments. AC acknowledges the
- 3 UPES Seed grant (UPES/R&D/SoAE/25062025/23)
- 4 for partially supporting this research. The research of
- 5 A.C., S.H., and S.S.H. were supported by the Cana-
- 6 dian Space Agency (CSA) and the Natural Sciences
- 7 and Engineering Research Council of Canada (NSERC)
- 8 through the Discovery Grants and the Canada Research
- 9 Chairs programs. The Basic Science Research Pro-
- 10 gram has supported K.H. through the National Research
- 11 Foundation of Korea (NRF), funded by the Ministry
- 12 of Education (2016R1A5A1013277 (K.H. and A.C.),
- 13 2020R1A2C1007219, and RS-2025-23323627 (K.H.)).
- 14 K.H. thanks Andrew Mummery for fruitful discussions.
- 15 AJ acknowledges support from the Fondecyt fellowship
- 16 (Proyecto 3230303). Research work at the Physical Re-
- 17 search Laboratory, Ahmedabad, is funded by the De-
- 18 partment of Space, Government of India. This re-
- 19 search has made use of data and/or software provided by
- 20 the High Energy Astrophysics Science Archive Research
- 21 Center (HEASARC), which is a service of the Astro-
- 22 physics Science Division at NASA/GSFC and the High
- 23 Energy Astrophysics Division of the Smithsonian As-
- 24 trophysical Observatory. This research has made use of
- 25 the NASA/IPAC Extragalactic Database (NED), which
- 26 is operated by the Jet Propulsion Laboratory, Califor-
- 27 nia Institute of Technology, under contract with the Na-
- 28 tional Aeronautics and Space Administration. This re-
- 29 search has made use of the SIMBAD database, operated
- 30 at CDS, Strasbourg, France.

REFERENCES

- Abramowicz, M., Jaroszynski, M., & Sikora, M. 1978, *A&A*, 63, 221
- Abramowicz, M. A., Calvani, M., & Nobili, L. 1980, *ApJ*, 242, 772, doi: [10.1086/158512](https://doi.org/10.1086/158512)
- Alexander, K. D., van Velzen, S., Horesh, A., & Zauderer, B. A. 2020, *Space Sci Rev*, 216, 81, doi: [10.1007/s11214-020-00702-w](https://doi.org/10.1007/s11214-020-00702-w)
- Alexander, T. 1997, in *Astronomical Time Series*, ed. D. Maoz, A. Sternberg, & E. M. Leibowitz (Dordrecht: Springer Netherlands), 163–166
- Alston, W. N., Parker, M. L., Markevičiūtė, J., et al. 2015, *MNRAS*, 449, 467, doi: [10.1093/mnras/stv351](https://doi.org/10.1093/mnras/stv351)
- Alston, W. N., Fabian, A. C., Kara, E., et al. 2020, *Nature Astronomy*, 4, 597, doi: [10.1038/s41550-019-1002-x](https://doi.org/10.1038/s41550-019-1002-x)
- Andreoni, I., Coughlin, M. W., Perley, D. A., et al. 2022, *Nature*, 612, 430, doi: [10.1038/s41586-022-05465-8](https://doi.org/10.1038/s41586-022-05465-8)
- Arnaud, K. A. 1996, in *Astronomical Society of the Pacific Conference Series*, Vol. 101, *Astronomical Data Analysis Software and Systems V*, ed. G. H. Jacoby & J. Barnes, 17
- Arnaud, K. A., Branduardi-Raymont, G., Culhane, J. L., et al. 1985, *MNRAS*, 217, 105, doi: [10.1093/mnras/217.1.105](https://doi.org/10.1093/mnras/217.1.105)
- Ashton, D. I., & Middleton, M. J. 2021, *MNRAS*, 501, 5478, doi: [10.1093/mnras/staa4024](https://doi.org/10.1093/mnras/staa4024)
- Bade, N., Komossa, S., & Dahlem, M. 1996, *A&A*, 309, L35
- Bennett, C. L., Halpern, M., Hinshaw, G., et al. 2003, *ApJS*, 148, 1, doi: [10.1086/377253](https://doi.org/10.1086/377253)
- Berger, E., Zauderer, A., Pooley, G. G., et al. 2012, *ApJ*, 748, 36, doi: [10.1088/0004-637X/748/1/36](https://doi.org/10.1088/0004-637X/748/1/36)
- Blandford, R., Meier, D., & Readhead, A. 2019, *ARA&A*, 57, 467, doi: [10.1146/annurev-astro-081817-051948](https://doi.org/10.1146/annurev-astro-081817-051948)
- Bloom, J. S., Butler, N. R., Cenko, S. B., & Perley, D. A. 2011a, *GRB Coordinates Network*, 11847, 1
- Bloom, J. S., Giannios, D., Metzger, B. D., et al. 2011b, *Science*, 333, 203, doi: [10.1126/science.1207150](https://doi.org/10.1126/science.1207150)
- Brown, G. C., Levan, A. J., Stanway, E. R., et al. 2015, *MNRAS*, 452, 4297, doi: [10.1093/mnras/stv1520](https://doi.org/10.1093/mnras/stv1520)
- Burrows, D. N., Hill, J. E., Nousek, J. A., et al. 2005, *SSRv*, 120, 165, doi: [10.1007/s11214-005-5097-2](https://doi.org/10.1007/s11214-005-5097-2)
- Burrows, D. N., Kennea, J. A., Ghisellini, G., et al. 2011, *Nature*, 476, 421, doi: [10.1038/nature10374](https://doi.org/10.1038/nature10374)
- Caiazzo, I., Belloni, T., Cackett, E., et al. 2019, *Unveiling the secrets of black holes and neutron stars with high-throughput, high-energy resolution X-ray spectroscopy*, Zenodo, doi: [10.5281/zenodo.3824441](https://doi.org/10.5281/zenodo.3824441)
- Cash, W. 2003, *Experimental Astronomy*, 16, 91, doi: [10.1007/s10686-004-2523-5](https://doi.org/10.1007/s10686-004-2523-5)
- Cash, W., Shipley, A., Osterman, S., & Joy, M. 2000, *Nature*, 407, 160, doi: [10.1038/35025009](https://doi.org/10.1038/35025009)
- Cendes, Y., Alexander, K. D., Berger, E., et al. 2021, *The Astrophysical Journal*, 919, 127, doi: [10.3847/1538-4357/ac110a](https://doi.org/10.3847/1538-4357/ac110a)
- Cendes, Y., Wijers, R. A. M. J., Swinbank, J. D., et al. 2014, *arXiv e-prints*, arXiv:1412.3986. <https://arxiv.org/abs/1412.3986>
- Cenko, S. B., Krimm, H. A., Horesh, A., et al. 2012, *ApJ*, 753, 77, doi: [10.1088/0004-637X/753/1/77](https://doi.org/10.1088/0004-637X/753/1/77)
- Chakrabarti, S., & Titarchuk, L. G. 1995, *ApJ*, 455, 623, doi: [10.1086/176610](https://doi.org/10.1086/176610)
- Chakrabarti, S. K. 1985a, *ApJ*, 288, 1, doi: [10.1086/162755](https://doi.org/10.1086/162755)
- . 1985b, *ApJ*, 288, 7, doi: [10.1086/162756](https://doi.org/10.1086/162756)
- Chakraborty, J., Masterson, M., Mummery, A., et al. 2026, *X-ray Spectral-Timing Properties of Tidal Disruption Events*. <https://arxiv.org/abs/2602.16868>
- Chatterjee, A. 2018, in *Exploring the Universe: From Near Space to Extra-Galactic*, ed. B. Mukhopadhyay & S. Sasmal (Cham: Springer International Publishing), 29–38
- Chatterjee, A., Chakrabarti, S. K., & Ghosh, H. 2017, *MNRAS*, 465, 3902, doi: [10.1093/mnras/stw2975](https://doi.org/10.1093/mnras/stw2975)
- Chatterjee, A., Chakrabarti, S. K., Ghosh, H., & Garain, S. K. 2018, *MNRAS*, 478, 3356, doi: [10.1093/mnras/sty1054](https://doi.org/10.1093/mnras/sty1054)
- Chatterjee, A., Dutta, B. G., Nandi, P., & Chakrabarti, S. K. 2020, *MNRAS*, 497, 4222, doi: [10.1093/mnras/staa2263](https://doi.org/10.1093/mnras/staa2263)
- Cruise, M., Guainazzi, M., Aird, J., et al. 2025, *Nature Astronomy*, 9, 36, doi: [10.1038/s41550-024-02416-3](https://doi.org/10.1038/s41550-024-02416-3)
- De Colle, F., & Lu, W. 2020, *NewAR*, 89, 101538, doi: [10.1016/j.newar.2020.101538](https://doi.org/10.1016/j.newar.2020.101538)
- Done, C., Davis, S. W., Jin, C., Blaes, O., & Ward, M. 2012, *MNRAS*, 420, 1848, doi: [10.1111/j.1365-2966.2011.19779.x](https://doi.org/10.1111/j.1365-2966.2011.19779.x)
- Donley, J. L., Brandt, W. N., Eracleous, M., & Boller, T. 2002, *AJ*, 124, 1308, doi: [10.1086/342280](https://doi.org/10.1086/342280)
- Edelson, R., Griffiths, G., Markowitz, A., et al. 2001, *ApJ*, 554, 274, doi: [10.1086/321332](https://doi.org/10.1086/321332)
- Edelson, R., & Malkan, M. 2012, *ApJ*, 751, 52, doi: [10.1088/0004-637X/751/1/52](https://doi.org/10.1088/0004-637X/751/1/52)
- Edelson, R., Turner, T. J., Pounds, K., et al. 2002, *ApJ*, 568, 610, doi: [10.1086/323779](https://doi.org/10.1086/323779)
- Edelson, R. A., Alexander, T., Crenshaw, D. M., et al. 1996, *ApJ*, 470, 364, doi: [10.1086/177872](https://doi.org/10.1086/177872)
- Eracleous, M., Livio, M., Halpern, J. P., & Storchi-Bergmann, T. 1995, *ApJ*, 438, 610, doi: [10.1086/175104](https://doi.org/10.1086/175104)

- Espinasse, M., Corbel, S., Kaaret, P., et al. 2020, *ApJL*, 895, L31, doi: [10.3847/2041-8213/ab88b6](https://doi.org/10.3847/2041-8213/ab88b6)
- Evans, P. A., Beardmore, A. P., Page, K. L., et al. 2009, *MNRAS*, 397, 1177, doi: [10.1111/j.1365-2966.2009.14913.x](https://doi.org/10.1111/j.1365-2966.2009.14913.x)
- Event Horizon Telescope Collaboration, Akiyama, K., Albetosa-Ruiz, E., et al. 2025, *A&A*, 704, A91, doi: [10.1051/0004-6361/202555855](https://doi.org/10.1051/0004-6361/202555855)
- Fabian, A. C., & George, I. M. 1991, in *Iron Line Diagnostics in X-ray Sources*, ed. A. Treves, G. C. Perola, & L. Stella (Berlin, Heidelberg: Springer Berlin Heidelberg), 167–176, doi: [10.1007/978-3-540-47583-5_13](https://doi.org/10.1007/978-3-540-47583-5_13)
- Foreman-Mackey, D., Hogg, D. W., Lang, D., & Goodman, J. 2013, *PASP*, 125, 306, doi: [10.1086/670067](https://doi.org/10.1086/670067)
- Fukue, J. 1982, *PASJ*, 34, 163, doi: [10.1093/pasj/34.2.163](https://doi.org/10.1093/pasj/34.2.163)
- Galeev, A. A., Rosner, R., & Vaiana, G. S. 1979, *ApJ*, 229, 318, doi: [10.1086/156957](https://doi.org/10.1086/156957)
- Gandhi, P. 2023, arXiv e-prints, arXiv:2310.15215, doi: [10.48550/arXiv.2310.15215](https://doi.org/10.48550/arXiv.2310.15215)
- Gendreau, K. C., Arzoumanian, Z., & Okajima, T. 2012, in *Society of Photo-Optical Instrumentation Engineers (SPIE) Conference Series*, Vol. 8443, *Space Telescopes and Instrumentation 2012: Ultraviolet to Gamma Ray*, ed. T. Takahashi, S. S. Murray, & J.-W. A. den Herder, 844313, doi: [10.1117/12.926396](https://doi.org/10.1117/12.926396)
- Gendreau, K. C., Cash, W. C., Shipley, A. F., & White, N. E. 2004, in *Society of Photo-Optical Instrumentation Engineers (SPIE) Conference Series*, Vol. 5168, *Optics for EUV, X-Ray, and Gamma-Ray Astronomy*, ed. O. Citterio & S. L. O'Dell, 420–434, doi: [10.1117/12.506198](https://doi.org/10.1117/12.506198)
- Gezari, S. 2021, arXiv e-prints, arXiv:2104.14580, <https://arxiv.org/abs/2104.14580>
- Gierliński, M., Middleton, M., Ward, M., & Done, C. 2008, *Nature*, 455, 369, doi: [10.1038/nature07277](https://doi.org/10.1038/nature07277)
- González-Rodríguez, A., Castro-Tirado, A. J., Guerrero, M. A., & Castellón, A. 2014, in *Revista Mexicana de Astronomía y Astrofísica Conference Series*, Vol. 45, *Revista Mexicana de Astronomía y Astrofísica Conference Series*, 73. <https://arxiv.org/abs/1402.4057>
- Guillochon, J., & Ramirez-Ruiz, E. 2013, *ApJ*, 767, 25, doi: [10.1088/0004-637X/767/1/25](https://doi.org/10.1088/0004-637X/767/1/25)
- Haardt, F., & Maraschi, L. 1991, *ApJL*, 380, L51, doi: [10.1086/186171](https://doi.org/10.1086/186171)
- Hayasaki, K. 2021, *Nature Astronomy*, 5, 436, doi: [10.1038/s41550-021-01309-z](https://doi.org/10.1038/s41550-021-01309-z)
- Hayasaki, K., Stone, N., & Loeb, A. 2013, *MNRAS*, 434, 909, doi: [10.1093/mnras/stt871](https://doi.org/10.1093/mnras/stt871)
- . 2016, *MNRAS*, 461, 3760, doi: [10.1093/mnras/stw1387](https://doi.org/10.1093/mnras/stw1387)
- Hayasaki, K., Zhong, S., Li, S., Berczik, P., & Spurzem, R. 2018, *ApJ*, 855, 129, doi: [10.3847/1538-4357/aab0a5](https://doi.org/10.3847/1538-4357/aab0a5)
- Heyl, J., Caiazzo, I., Hoffman, K., et al. 2019, in *Bulletin of the American Astronomical Society*, Vol. 51, 175
- Jana, A., Debnath, D., Chakrabarti, S. K., Mondal, S., & Molla, A. A. 2016, *ApJ*, 819, 107, doi: [10.3847/0004-637X/819/2/107](https://doi.org/10.3847/0004-637X/819/2/107)
- Jana, A., Kumari, N., Nandi, P., et al. 2021, *MNRAS*, 507, 687, doi: [10.1093/mnras/stab2155](https://doi.org/10.1093/mnras/stab2155)
- Jaroszynski, M. 1986, *MNRAS*, 220, 869, doi: [10.1093/mnras/220.4.869](https://doi.org/10.1093/mnras/220.4.869)
- Jiang, Y.-F., & Dai, L. 2024, arXiv e-prints, arXiv:2408.16856, doi: [10.48550/arXiv.2408.16856](https://doi.org/10.48550/arXiv.2408.16856)
- Jiang, Y.-F., Stone, J. M., & Davis, S. W. 2019, *ApJ*, 880, 67, doi: [10.3847/1538-4357/ab29ff](https://doi.org/10.3847/1538-4357/ab29ff)
- Kara, E., Miller, J. M., Reynolds, C., & Dai, L. 2016, *Nature*, 535, 388, doi: [10.1038/nature18007](https://doi.org/10.1038/nature18007)
- Kara, E., Steiner, J. F., Fabian, A. C., et al. 2019, *Nature*, 565, 198, doi: [10.1038/s41586-018-0803-x](https://doi.org/10.1038/s41586-018-0803-x)
- Kawaguchi, T. 2003, *ApJ*, 593, 69, doi: [10.1086/376404](https://doi.org/10.1086/376404)
- Komossa, S. 2017, *Astronomische Nachrichten*, 338, 256, doi: [10.1002/asna.201713339](https://doi.org/10.1002/asna.201713339)
- Kormendy, J., & Ho, L. C. 2013, *ARA&A*, 51, 511, doi: [10.1146/annurev-astro-082708-101811](https://doi.org/10.1146/annurev-astro-082708-101811)
- Kormendy, J., & Richstone, D. 1995, *ARA&A*, 33, 581, doi: [10.1146/annurev.aa.33.090195.003053](https://doi.org/10.1146/annurev.aa.33.090195.003053)
- Koss, M., Aftab, N., Allen, S. W., et al. 2025, arXiv e-prints, arXiv:2511.00253, doi: [10.48550/arXiv.2511.00253](https://doi.org/10.48550/arXiv.2511.00253)
- Kozłowski, M., Jaroszynski, M., & Abramowicz, M. A. 1978, *A&A*, 63, 209
- Lei, W.-H., Yuan, Q., Zhang, B., & Wang, D. 2016, *ApJ*, 816, 20, doi: [10.3847/0004-637X/816/1/20](https://doi.org/10.3847/0004-637X/816/1/20)
- Levan, A. J., Tanvir, N. R., Cenko, S. B., et al. 2011, *Science*, 333, 199, doi: [10.1126/science.1207143](https://doi.org/10.1126/science.1207143)
- Levan, A. J., Tanvir, N. R., Brown, G. C., et al. 2016, *ApJ*, 819, 51, doi: [10.3847/0004-637X/819/1/51](https://doi.org/10.3847/0004-637X/819/1/51)
- Lin, D., Irwin, J. A., Godet, O., Webb, N. A., & Barret, D. 2013, *ApJL*, 776, L10, doi: [10.1088/2041-8205/776/1/L10](https://doi.org/10.1088/2041-8205/776/1/L10)
- Liu, B. F., Mineshige, S., & Shibata, K. 2002, *ApJL*, 572, L173, doi: [10.1086/341877](https://doi.org/10.1086/341877)
- Lodato, G., & Rossi, E. M. 2011, *MNRAS*, 410, 359, doi: [10.1111/j.1365-2966.2010.17448.x](https://doi.org/10.1111/j.1365-2966.2010.17448.x)
- Madau, P. 1988, *ApJ*, 327, 116, doi: [10.1086/166175](https://doi.org/10.1086/166175)
- Magorrian, J., & Tremaine, S. 1999, *MNRAS*, 309, 447, doi: [10.1046/j.1365-8711.1999.02853.x](https://doi.org/10.1046/j.1365-8711.1999.02853.x)
- Mangano, V., Burrows, D. N., Sbarufatti, B., & Cannizzo, J. K. 2016, *ApJ*, 817, 103, doi: [10.3847/0004-637X/817/2/103](https://doi.org/10.3847/0004-637X/817/2/103)

- Martocchia, A., & Matt, G. 1996, *MNRAS*, 282, L53, doi: [10.1093/mnras/282.4.L53](https://doi.org/10.1093/mnras/282.4.L53)
- McClintock, J. E., Remillard, R. A., Rupen, M. P., et al. 2009, *ApJ*, 698, 1398, doi: [10.1088/0004-637X/698/2/1398](https://doi.org/10.1088/0004-637X/698/2/1398)
- Merloni, A., Predehl, P., Becker, W., et al. 2012, arXiv e-prints, arXiv:1209.3114, <https://arxiv.org/abs/1209.3114>
- Merloni, A., Dwelly, T., Salvato, M., et al. 2015, *MNRAS*, 452, 69, doi: [10.1093/mnras/stv1095](https://doi.org/10.1093/mnras/stv1095)
- Miniutti, G., & Fabian, A. C. 2004, *MNRAS*, 349, 1435, doi: [10.1111/j.1365-2966.2004.07611.x](https://doi.org/10.1111/j.1365-2966.2004.07611.x)
- Mirabel, I. F., & Rodríguez, L. F. 1994, *Nature*, 371, 46, doi: [10.1038/371046a0](https://doi.org/10.1038/371046a0)
- Mummery, A., & Balbus, S. A. 2021, *MNRAS*, 504, 4730, doi: [10.1093/mnras/stab1184](https://doi.org/10.1093/mnras/stab1184)
- Mushotzky, R., & AXIS Team. 2019, in *LPI Contributions*, Vol. 2135, *The Space Astrophysics Landscape for the 2020s and Beyond*, ed. Moores J. E., King P. L., Smith C. L., Martinez G. M., Newman C. E., Guzewich S. D., Meslin P. -Y., Webster C. R., Mahaffy P. R., Atreya S. K., & Schuerger A. C., 5025
- Nandra, K., George, I. M., Mushotzky, R. F., Turner, T. J., & Yaqoob, T. 1997, *ApJ*, 476, 70, doi: [10.1086/303600](https://doi.org/10.1086/303600)
- Narayan, R., Igumenshchev, I. V., & Abramowicz, M. A. 2003, *PASJ*, 55, L69, doi: [10.1093/pasj/55.6.L69](https://doi.org/10.1093/pasj/55.6.L69)
- Nikołajuk, M., & Walter, R. 2013, *A&A*, 552, A75, doi: [10.1051/0004-6361/201220664](https://doi.org/10.1051/0004-6361/201220664)
- Paczynski, B., & Wiita, P. J. 1980, *A&A*, 88, 23
- Park, G., & Hayasaki, K. 2020, *ApJ*, 900, 3, doi: [10.3847/1538-4357/ab9ebb](https://doi.org/10.3847/1538-4357/ab9ebb)
- Pasham, D. R., Remillard, R. A., Fragile, P. C., et al. 2019, *Science*, 363, 531, doi: [10.1126/science.aar7480](https://doi.org/10.1126/science.aar7480)
- Patra, D., Chatterjee, A., Dutta, B. G., Chakrabarti, S. K., & Nandi, P. 2019, *ApJ*, 886, 137, doi: [10.3847/1538-4357/ab4c34](https://doi.org/10.3847/1538-4357/ab4c34)
- Peterson, B. M., Ferrarese, L., Gilbert, K. M., et al. 2004, *ApJ*, 613, 682, doi: [10.1086/423269](https://doi.org/10.1086/423269)
- Rees, M. J. 1988, *Nature*, 333, 523, doi: [10.1038/333523a0](https://doi.org/10.1038/333523a0)
- Rees, M. J., Begelman, M. C., Blandford, R. D., & Phinney, E. S. 1982, *Nature*, 295, 17, doi: [10.1038/295017a0](https://doi.org/10.1038/295017a0)
- Reis, R. C., Miller, J. M., Reynolds, M. T., et al. 2012, *Science*, 337, 949, doi: [10.1126/science.1223940](https://doi.org/10.1126/science.1223940)
- Reynolds, C. S., Kara, E. A., Mushotzky, R. F., et al. 2023, arXiv e-prints, arXiv:2311.00780, doi: [10.48550/arXiv.2311.00780](https://doi.org/10.48550/arXiv.2311.00780)
- Ricci, C., Kara, E., Loewenstein, M., et al. 2020, *ApJL*, 898, L1, doi: [10.3847/2041-8213/ab91a1](https://doi.org/10.3847/2041-8213/ab91a1)
- Ricci, C., Loewenstein, M., Kara, E., et al. 2021, arXiv e-prints, arXiv:2102.05666, <https://arxiv.org/abs/2102.05666>
- Rossi, E. M., Stone, N. C., Law-Smith, J. A. P., et al. 2021, *SSRv*, 217, 40, doi: [10.1007/s11214-021-00818-7](https://doi.org/10.1007/s11214-021-00818-7)
- Safi-Harb, S., Burdge, K. B., Bodaghee, A., et al. 2023, arXiv e-prints, arXiv:2311.07673, doi: [10.48550/arXiv.2311.07673](https://doi.org/10.48550/arXiv.2311.07673)
- Saxton, C. J., Soria, R., Wu, K., & Kuin, N. P. M. 2012, *MNRAS*, 422, 1625, doi: [10.1111/j.1365-2966.2012.20739.x](https://doi.org/10.1111/j.1365-2966.2012.20739.x)
- Seifina, E., Titarchuk, L., & Virgili, E. 2017, *A&A*, 607, A38, doi: [10.1051/0004-6361/201730869](https://doi.org/10.1051/0004-6361/201730869)
- Sikora, M. 1981, *MNRAS*, 196, 257, doi: [10.1093/mnras/196.2.257](https://doi.org/10.1093/mnras/196.2.257)
- Singh, K. P., Garmire, G. P., & Nousek, J. 1985, *ApJ*, 297, 633, doi: [10.1086/163560](https://doi.org/10.1086/163560)
- Stein, R., Velzen, S. v., Kowalski, M., et al. 2021, *Nature Astronomy*, 5, 510, doi: [10.1038/s41550-020-01295-8](https://doi.org/10.1038/s41550-020-01295-8)
- Sun, H., Zhang, B., & Li, Z. 2015, *ApJ*, 812, 33, doi: [10.1088/0004-637X/812/1/33](https://doi.org/10.1088/0004-637X/812/1/33)
- Tanaka, Y., Nandra, K., Fabian, A. C., et al. 1995, *Nature*, 375, 659, doi: [10.1038/375659a0](https://doi.org/10.1038/375659a0)
- Tashiro, M., Maejima, H., Toda, K., et al. 2018, in *Space Telescopes and Instrumentation 2018: Ultraviolet to Gamma Ray*, ed. J.-W. A. den Herder, S. Nikzad, & K. Nakazawa, Vol. 10699, *International Society for Optics and Photonics (SPIE)*, 520 – 531, doi: [10.1117/12.2309455](https://doi.org/10.1117/12.2309455)
- Tchekhovskoy, A., Metzger, B. D., Giannios, D., & Kelley, L. Z. 2014, *MNRAS*, 437, 2744, doi: [10.1093/mnras/stt2085](https://doi.org/10.1093/mnras/stt2085)
- Ulmer, A. 1997, arXiv e-prints, astro, doi: [10.48550/arXiv.astro-ph/9708265](https://doi.org/10.48550/arXiv.astro-ph/9708265)
- Uttley et al., P. 2020, in *Society of Photo-Optical Instrumentation Engineers (SPIE) Conference Series*, Vol. 11444, *Society of Photo-Optical Instrumentation Engineers (SPIE) Conference Series*, 114441E, doi: [10.1117/12.2562523](https://doi.org/10.1117/12.2562523)
- Vaughan, S., Edelson, R., Warwick, R. S., & Uttley, P. 2003, *MNRAS*, 345, 1271, doi: [10.1046/j.1365-2966.2003.07042.x](https://doi.org/10.1046/j.1365-2966.2003.07042.x)
- Vaughan, S., & Uttley, P. 2005, *MNRAS*, 362, 235, doi: [10.1111/j.1365-2966.2005.09296.x](https://doi.org/10.1111/j.1365-2966.2005.09296.x)
- . 2006, *Advances in Space Research*, 38, 1405, doi: [10.1016/j.asr.2005.02.064](https://doi.org/10.1016/j.asr.2005.02.064)
- Walter, R., Bordas, P., Bozzo, E., et al. 2011, *The Astronomer's Telegram*, 3108, 1
- Wang, J., & Merritt, D. 2004, *ApJ*, 600, 149, doi: [10.1086/379767](https://doi.org/10.1086/379767)

Weaver, K. A., Cann, J. M., Pfeifle, R., et al. 2026, arXiv e-prints, arXiv:2601.20823, doi: [10.48550/arXiv.2601.20823](https://doi.org/10.48550/arXiv.2601.20823)

Zauderer, B. A., Berger, E., Margutti, R., et al. 2013, ApJ, 767, 152, doi: [10.1088/0004-637X/767/2/152](https://doi.org/10.1088/0004-637X/767/2/152)

Zauderer, B. A., Berger, E., Soderberg, A. M., et al. 2011, Nature, 476, 425, doi: [10.1038/nature10366](https://doi.org/10.1038/nature10366)

Zhong, S., Hayasaki, K., Li, S., Berczik, P., & Spurzem, R. 2023, ApJ, 959, 19, doi: [10.3847/1538-4357/ad0122](https://doi.org/10.3847/1538-4357/ad0122)